Mon. Not. R. Astron. Soc. **374,** 305–322 (2007) doi:10.1111/j.1365-2966.2006.11149.x

On the effects of coherent structures on higher order moments in models of solar and stellar surface convection

F. Kupka[1]★ and F. J. Robinson[2,3]

[1]*Max-Planck-Institute for Astrophysics, Karl-Schwarzschild-Str. 1, 85741 Garching, Germany*
[2]*Department of Geology and Geophysics, Yale University, Box 208109, New Haven, CT 06520-8109, USA*
[3]*Astronomy Department, Yale University, Box 208101, New Haven, CT 06520-8101, USA*

Accepted 2006 October 3. Received 2006 September 29; in original form 2006 June 21

ABSTRACT

Non-local models of stellar convection usually rely on the assumption that the transfer of convective heat flux, turbulent kinetic energy and related quantities can be described as a diffusion process or that the fourth-order moments of velocity and temperature fluctuations follow a Gaussian distribution (quasi-normal approximation). The latter is also assumed in models of solar p-mode excitation.

We have used realistic numerical simulations of solar granulation and of granulation in a K dwarf to test the quasi-normal approximation and several alternatives. For the superadiabatic layer of the Sun and for the quasi-adiabatic zone underneath, we find that the hypothesis of quasi-normality is a rather poor approximation. In the superadiabatic layer, it overestimates some of the fourth-order moments of vertical velocity and temperature by up to a factor of 2 while it underestimates them in the quasi-adiabatic layers by up to a factor of 3.5. The model proposed by Gryanik & Hartmann and Gryanik et al. reduces the discrepancies within the quasi-adiabatic zone to typically less than 30 per cent and is partially comparable and partially in better agreement with the simulation data than two earlier models by Grossman & Narayan. Simulation data for the K dwarf confirm these results. However, none of the proposed models works well in the superadiabatic layer nor in the photospheric layers above. For the Sun, we provide evidence that the fourth-order moments of horizontal velocity fields can be estimated to within about 30 per cent with the quasi-normal approximation despite the complexity of the horizontal flow. Comparing our results to those from solar simulations with idealized microphysics and with related studies of geophysical convection zones confirms our conclusions about the quasi-normal approximation and the new models.

The improvements come from including the effects of coherent structures (such as granules or plumes), while the limitations are tied to the transition regions or boundaries such as the rapid radiative cooling that occurs at the top of the convection zone. Incorporating the model of Gryanik & Hartmann and Gryanik et al. into non-local convection models may well produce a significant improvement in the modelling of convection or of solar-like p-mode excitation in the quasi-adiabatic part of convection zones. For application to entire convection zones, modifications are necessary which can account for the change in background properties of the convective medium near boundaries or transition regions.

Key words: convection – turbulence – Sun: atmosphere – Sun: interior – stars: atmospheres – stars: interiors.

1 INTRODUCTION

Convective heat transport and convective mixing are still a major source of uncertainty in the theory of stellar structure and evolution. Models currently used to describe these processes provide order of magnitude estimates and entail parameters which require case-dependent adjustments. One of the main shortcomings of these models is the assumption of locality. It presupposes that kinetic energy, heat flux and other quantities at a given radius in the star depend on the physical state of the star and on gradients of the mean structure at that radius alone. Another shortcoming is related to the

★E-mail: fk@mpa-garching.mpg.de

assumption of homogeneity and isotropy of the flow which is used in most of these models. Observations of solar surface granulation and numerical simulations of stellar convection have demonstrated that convection overshoots into stably stratified layers and is inhomogeneous and anisotropic, particularly in transition regions between stable and unstable stratification. None of these features is accounted for in standard local convection models (e.g. the mixing-length theory as defined in Böhm-Vitense 1958 or Cox & Giuli 1968, and also the models of Canuto & Mazzitelli 1991 and Canuto, Goldman & Mazzitelli 1996).

To overcome these difficulties, non-local models of stellar convection have been proposed. As with the standard models, the non-local models cannot be derived from the basic hydrodynamical equations without introducing additional assumptions. Hydrodynamical moment equations are currently the most systematic approach for deriving such models. Their purpose is the prediction of ensemble averages of velocity, temperature and density – or more precisely, the computation of moments of the ensemble-averaged fluctuations of these fields around their mean values. For applications in stellar structure calculations, one-point averages are the most convenient, because they are just a function of location (and time). In this paper, we restrict ourselves to the discussion of one-point averages. The non-linearities in the hydrodynamical equations mean that the hierarchy of ensemble-averaged equations is unclosed so to obtain a finite number of moment equations requires additional closure approximations. These include geometrical approximations which result in averages that are functions of depth (or radius) and time and other approximations introduced by truncating the moment expansion at a certain order.

Most models of convection treat the non-local transfer as a diffusion process. In which case, the flux of a physical quantity can be approximated by the gradient of the transported quantity times a turbulent diffusivity. As an example, consider a second-order moment (SOM), the turbulent kinetic energy per unit mass

$$K = \frac{1}{2}\,\overline{q^2}, \quad \text{with} \quad \overline{q^2} = \overline{u^2} + \overline{v^2} + \overline{w^2}, \tag{1}$$

where u, v and w are the fluctuating parts of the three components of the instantaneous velocity, (v_x, v_y, v_z). The ensemble average of the latter is defined as $(\overline{v_x}, \overline{v_y}, \overline{v_z})$, thus $(v_x, v_y, v_z) = (\overline{v_x}, \overline{v_y}, \overline{v_z}) + (u, v, w)$. The flux of turbulent kinetic energy can be approximated as

$$F_z^{\rm k} \approx -(1/2)\,\overline{\rho}\,\kappa_{\rm t}\left(\partial\overline{q^2}/\partial z\right), \tag{2}$$

where $\overline{\rho}$ is the mean density. The turbulent diffusivity $\kappa_{\rm t}$ is computed from local properties of the flow which typically include $\overline{w^2}$ and a length-scale l or a time-scale τ to account for the influence of stratification, compressibility and domain size. For instance, one could use $\kappa_{\rm t} = [(\overline{w^2})^{0.5} l_{\rm t}]$, where $l_{\rm t} = \alpha H_{\rm p}$ is a mixing length based on the local pressure scaleheight $H_{\rm p}$. This approach is also known as the down-gradient approximation. Systematic derivations of convection models using this type of approximation have been suggested by Xiong (1980) and Kuhfuss (1986), but its ingredients have also been used by many others (see Canuto 1993, for a summary of such models). Unfortunately, down-gradient type models only work well for part of the convection zone even if adjustments to the turbulent diffusivities are made. Zeman & Lumley (1976) discussed the limitations of these models for the case of the planetary boundary layer (PBL) and proposed a more complete model, while Chan & Sofia (1996) used numerical simulations of deep compressible convection to show that several suggested gradient models of $\overline{w^3}$ were out by a factor of 2 or 3 over several pressure scaleheights. This was even after least-square optimization of an adjustable factor that had been placed in front of the turbulent diffusivity.

To avoid diffusion-type approximations, it has been suggested to consider the full dynamical equations for the third-order moments (TOMs). Astrophysical examples of this strategy include Canuto (1992, 1993, 1997), Grossman & Narayan (1993) and Xiong, Cheng & Deng (1997). These models are confronted with the closure problem for fourth-order moments (FOMs) and rely on the assumption that the FOMs of velocity and temperature fluctuations are Gaussian correlated (i.e. the quasi-normal approximation). While this idea is attractive due to its mathematical simplicity, there are also several caveats (see Section 3). The most well known among them originates from the possibility of violating physical realizability. Orszag (1970) proposed the concept of eddy damping to avoid that problem. In this approach, the dynamical equations of the TOMs are modified to ensure realizability whereas the FOMs themselves are left unaltered, i.e. during their derivation the quasi-normal approximation is still used for these models. Such methods have been used, e.g. in Canuto (1992, 1993, 1997).

An alternative to eddy damping methods is the direct improvement of the approximation used for the FOMs themselves. Gryanik & Hartmann (2002) proposed a new model for the FOMs of vertical velocity and temperature fluctuations. It is based on a two-scale mass-flux approach and has recently been extended by Gryanik et al. (2005) to include horizontal velocities and all cross-correlations to fourth order. In contrast to diffusion-type models or the quasi-normal approximation, the new model accounts for the fact that convection zones have a coherently structured large-scale flow (e.g. up- and downdrafts, plumes and granules) which plays a dominant role in non-local transport. Successful tests of the model based on aircraft data and numerical simulations of the PBL were presented in Gryanik & Hartmann (2002) and Gryanik et al. (2005). Losch (2004) used numerical simulations of convection in the ocean to investigate the model of Gryanik & Hartmann (2002) and Gryanik et al. (2005) and found good agreement with his simulation data. Moreover, preliminary tests based on numerical simulations indicate that the same improvements over the quasi-normal approximation should hold for the case of solar surface convection (Kupka 2005a). The model of Gryanik & Hartmann (2002) and Gryanik et al. (2005) has some similarities to earlier proposals by Grossman & Narayan (1993), but a direct comparison of all these models for the case of the Sun or another star has not yet been done.

The goal of this study is to find out how well these models represent FOMs for the case of surface convection in the Sun and in cool stars. What we want to know is how much they can improve non-local convection models and other applications which to date have had to rely on the quasi-normal approximation. For that reason, we use data from numerical simulations that have thoroughly been tested against observed solar data (reproducing solar-sized granules and p modes within a few microhertz of observed values) and independently performed simulations (see Section 2.1 and also the discussion in Kupka 2005b). Conceptually, they are large eddy simulations (LES), since they only resolve the scales that transport most of the kinetic energy (and heat) of the convective flow, a currently inevitable restriction for any simulation of stellar convection with realistic microphysics. For the quasi-adiabatic part of convection zones, the new models provide a significant improvement over the quasi-normal approximation which is found to be inadequate for the photosphere, superadiabatic layer and top few pressure scaleheights of the solar convection zone. The same results are found for a K dwarf. In Table 1, we present the extent of these different zones for both simulations in terms of pressure scaleheights (i.e. as

Table 1. Boundaries of different regions measured in $\ln P$ for the Sun and K dwarf simulations. Note that the pressure at the top and bottom of each simulation box will be different from the initial stellar models because of the effects of turbulent pressure and temperature fluctuations. The influence of the upper and lower boundaries on the convection statistics is small between Z_1 (the top of the convection zone defined as where $\nabla = \nabla_{\rm ad}$) and Z_3 (where $\nabla - \nabla_{\rm ad}$ is ∼0.5 per cent of its peak value). Both are about 1.5–2 pressure scaleheights away from the vertical boundaries of the box. The base of the superadiabatic layer is indicated by Z_2 which we define, where $\nabla - \nabla_{\rm ad}$ is ∼5 per cent of its peak value, since at that point its change with depth becomes small.

Model	Top	Z_1	Z_2	Z_3	Bottom
Sun	10.3	11.6	13.1	16	17.7
K dwarf	10.2	12.4	14.4	17	18.5

functions of $\ln P$). The upper boundary of the superadiabatic layer (Z_1) is defined by the physical condition of local stability (Schwarzschild criterion), while the lower one (Z_2) is located at the level at which $\nabla - \nabla_{\rm ad}$ is 5 per cent of its maximum value. The quasi-adiabatic stratification is influenced by the lower boundary only for layers below Z_3 which are neglected in most of our discussion.

The rest of the paper is laid out as follows. First, we give an outline of the numerical simulations (Section 2) followed by a description of the various models to be tested (Section 3). The results are then presented in Section 4 followed by a comparison with studies in related fields in Section 5. We end with a discussion of our results and conclusions (Section 6).

2 3D NUMERICAL SIMULATION OF SURFACE CONVECTION IN THE SUN AND A K DWARF

The 3D simulation of the Sun we have used for our study is case D in Robinson et al. (2003). This box has dimensions $2900 \times 2900 \times 3000$ km^3 on a $58 \times 58 \times 170$ grid.

A detailed one-dimensional (1D) evolutionary model, e.g. see Guenther (1994), provides the starting model for the 3D simulation. In particular, the low-temperature opacities of Alexander & Ferguson (1994) and the OPAL opacities and equation of state were used (Iglesias & Rogers 1996). Hydrogen and helium ionization, and the diffusion of both helium and heavy elements are included. The values of the parameters, X, Z and α, in the calibrated standard solar model (SSM) are $(X, Z, \alpha) = (0.7385, 0.0181, 2.02)$, where X and Y are the hydrogen and helium abundances by mass, $Z = 1 - X - Y$, and α is the ratio of mixing length to pressure scaleheight in the convection zone, required to match precisely the solar radius. Additional details of the numerical approach and physical assumptions are described in Robinson et al. (2003).

The simulation extends from a few hundred km above the photosphere down to a depth of about 2500 km below the visible surface (defined as where the optical depth is unity). This is about 7.5 pressure scaleheights in the thermally relaxed model. The box has periodic side walls and impenetrable top and bottom surfaces. A constant energy flux is fed into the base and a conducting top boundary is used. The flux is computed from the 1D stellar model, thus it is not arbitrary, but is the correct amount of energy flux the computation domain should transport outwards in a particular star. For the simulations of the solar case, this flux corresponds to a $T_{\rm eff}$ of 5777 K. Surface gravity g is taken to be 274 m s^{-2}, i.e. a (CGS units) $\log g$ of 4.4377 is assumed.

To get a thermally relaxed system in a reasonable amount of computer time, we use an implicit numerical scheme, ADISM (alternating direction implicit on a staggered mesh) developed by Chan & Wolff (1982). Careful attention was paid to the geometric size of the box. The domain was deep and wide enough to ensure the boundaries had minimal effect on the bulk of the overturning convective eddies (or on the flow statistics). The convection simulation is run using the ADISM code until it has reached a statistically steady state. One way of checking this is to compare the influx and outflux of the box. They should be within 5 per cent of each other. A snapshot of part of the velocity field from the solar simulation is shown as a vertical cut in Fig. 1. Red (light) arrows denote upward velocity vectors and blue (dark) arrows downward ones.

After the model has relaxed, the averages are computed over about 150 min of solar convection (about 20 granule turnover/lifetimes). This is a sufficiently long enough time for most quantities to converge (in general, all quantities were averaged over a time that was long enough for the averages to be independent of the integration time). However, even though some first- and second-order quantities may appear to have converged it does not mean that other higher order quantities have. For each statistical quantity presented in this paper, convergence was thoroughly checked by confirming that averaging over a longer time did not change the result. The only quantities which may benefit from longer averaging are skewness and kurtosis of horizontal velocities in the lower half of the simulation domain (this is discussed in Section 4.1).

To confirm that the results for the closure models are not just valid for the Sun, we ran a simulation of convection in a low-mass star. Numerical simulations for a 0.7 $M_\odot$ star have been performed, well in the range of K dwarfs. For this star, $(X, Z, \alpha) = (0.7, 0.018, 1.8)$, $T_{\rm eff}$ was taken to be 4609 K and the surface gravity was chosen to be about 449 m s^{-2} (i.e. a $\log g = 4.6523$ in CGS units) which corresponds to an age of $t \sim 6$ Gyr. The computational grid had $58 \times 58 \times 180$ grid points representing a box of $2700 \times 2700 \times 1350$ km^3. Statistical convergence was confirmed for all quantities apart from the kurtosis of temperature in the two lowermost pressure scaleheights (see Sections 3.1 and 4.1).

2.1 Testing the simulations against observations and other solar simulations

By incorporating averages computed from the 3D simulation into a 1D stellar model, it was possible to produce solar surface eigenfrequencies (p-modes) that were within 5 μHz of the observed frequencies (Robinson et al. 2003) and granules with a mean diameter close to the observed value. In addition, the structure of the superadiabatic layer and rms vertical velocities in our simulation are almost identical to those in the solar surface simulations by Rosenthal et al. (1999) and Asplund et al. (2000). Thus we have a lot of confidence in our simulation data as a testsuite for comparing the respective closure approximations (see also the comparison in Kupka 2005b).

3 MODELS FOR FOMs

Each of the convection models suggested by Canuto (1992, 1993, 1997), Canuto & Dubovikov (1998) and Xiong et al. (1997) requires the solution of differential equations for SOMs of velocity and temperature, which are ultimately closed using approximations for the FOMs. However, the ensemble averages used in these models are not identical. Canuto (1997) accounts for compressibility through density-weighted (Favre) averages ($\overline{\rho v_z^2}/\overline{\rho}$, etc.), while Xiong et al. (1997) use a normalization relative to local temperature (θ/T instead

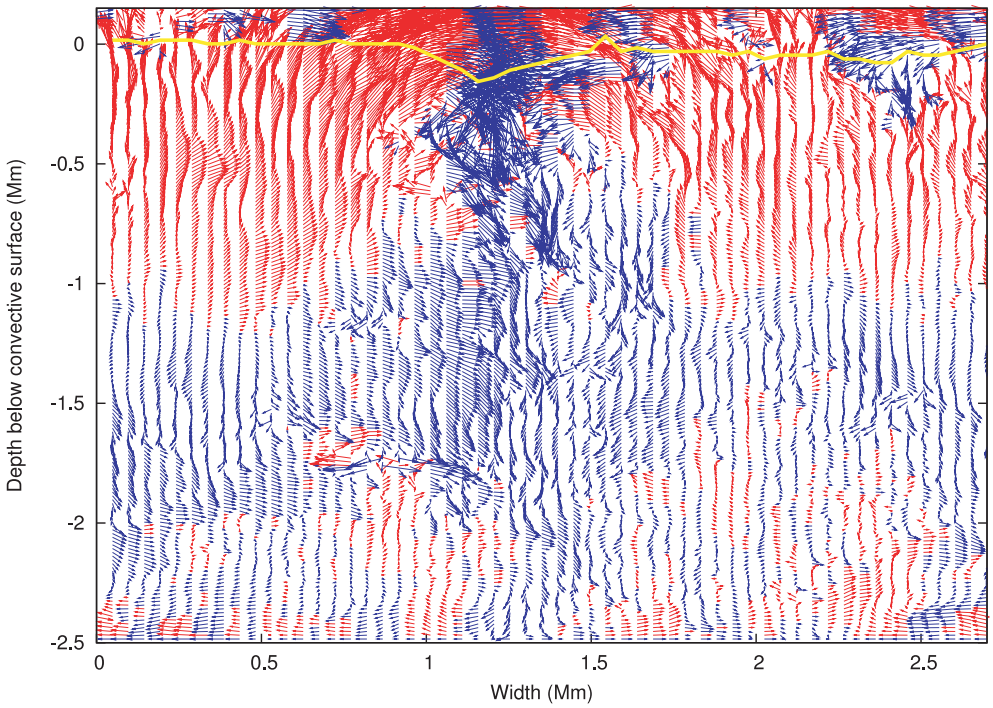

Figure 1. A snapshot of the velocity field in an arbitrary vertical plane taken from the 3D simulation of the Sun. The red (light) velocity vectors have an upward component and the blue (dark) ones a downward component. The optical surface (defined by unit optical depth) is indicated as a thick (yellow) line near the top.

of θ) for all moments which depend on temperature. The ensemble averaging we use is the same as in Canuto (1992, 1993), Canuto & Dubovikov (1998) and Grossman & Narayan (1993), and described below (see also Sections 1 and 2): the fluctuations of temperature, θ, and vertical velocity, w, around their mean values $\overline{T}$ and $\overline{v_z}$ are related to the instantaneous temperature T and vertical velocity v_z through

$$T = \overline{T} + \theta \quad \text{and} \quad v_z = \overline{v_z} + w. \tag{3}$$

Hence, there is no local weighting of the ensemble-averaged quantities. The ensemble average, denoted by the overbar, can be approximately computed from a numerical simulation by performing a time average for each physical quantity. The quantities averaged this way are horizontal averages performed at one instant in time (see Section 2 about the convergence of such averages). Assuming that turbulent convective flows are quasi-ergodic and thus that any thermally relaxed initial physical state of the basic variables is appropriate to start visiting all physical realizations of these variables with their correct probability, we can thus compute ensemble averages from the simulations. The main limitation of this process is the uncertainties introduced by the finite grid size, simulation box and averaging time as well as uncertainties introduced by the subgrid scale model employed to parametrize the unresolved scales. An estimate of these effects is briefly discussed in Section 2 and in more detail in Robinson et al. (2003).

The SOMs which appear in the aforementioned models are

$$K, \quad \overline{\theta^2}, \quad J = \overline{w\theta} \quad \text{and} \quad \overline{w^2}, \tag{4}$$

where K is the turbulent kinetic energy defined in equation (1). The dynamical equations for equation (4) require computation of the turbulent fluxes of K, $\overline{\theta^2}$, J and $\overline{w^2}$ (Canuto 1992):

$$\overline{q^2 w}, \quad \overline{w\theta^2}, \quad \overline{w^2\theta} \quad \text{and} \quad \overline{w^3}. \tag{5}$$

If these quantities are computed without using the diffusion approximation (see Section 1), then one needs to solve the full dynamical equations. This requires computation of the turbulent fluxes of equation (5):

$$\overline{q^2 w^2}, \quad \overline{w^2\theta^2}, \quad \overline{w^3\theta} \quad \text{and} \quad \overline{w^4} \tag{6}$$

(see again Canuto 1992). Equations (5) and (6) mention only some of the TOMs and FOMs which appear in the dynamical equations for equations (4) and (5). Additional lower order moments may be required depending on the model (or avoided, such as $\overline{q^2 w}$ and $\overline{q^2 w^2}$, if assumptions on anisotropy are made).

It is convenient to define some auxiliary quantities which are used to formulate the FOM models. The rms average of vertical velocity and temperature fluctuations as well as their cross-correlation are defined by

$$\sigma_w = \overline{w^2}^{1/2}, \quad \sigma_\theta = \overline{\theta^2}^{1/2}, \quad C_{w\theta} = \frac{\overline{w\theta}}{\sigma_w\,\sigma_\theta}. \tag{7}$$

The skewnesses of vertical velocity and temperature are

$$S_w = \overline{w^3}/\overline{w^2}^{3/2} \quad \text{and} \quad S_\theta = \overline{\theta^3}/\overline{\theta^2}^{3/2}, \tag{8}$$

while the kurtoses are

$$K_w = \frac{\overline{w^4}}{\sigma_w^4} \quad \text{and} \quad K_\theta = \frac{\overline{\theta^4}}{\sigma_\theta^4}. \tag{9}$$

Physically, the skewness provides a simple measure for the asymmetry of the probabilities of velocity being directed up- or downwards and of temperature being hotter or colder than average. Positive values of S_w signify upflows with a smaller area than the downflows while $S_w < 0$ implies the opposite. The reason for this is that $\overline{w^3}$ gives more weight to higher velocities which due to mass conservation preferentially occur in the component covering a smaller horizontal area. Mass-flux models provide a mapping (cf. Canuto

& Dubovikov 1998; Gryanik & Hartmann 2002) between velocity skewness and filling factor (fraction of horizontal area covered by upflows), although the exact relation between the two is complicated. A similar correlation exists for temperature (S_θ) and the area covered by hot or cold fluid. They are not necessarily correlated with S_w and the filling factor (see Section 3.3). The kurtoses K_w and K_θ provide a measure for the likeliness of fluctuations to occur which are much larger than the rms average (σ_w and σ_θ). A large kurtosis combined with a small skewness implies that the flow has strong or at least frequent *intermittent* events. These may be caused, for instance, by strong individual downdrafts and also by large fluctuations within the downdrafts. In this case, the distribution functions for the probabilities of deviations of local velocities and temperatures from their mean are characterized by long tails (compared to a Gaussian distribution). A small value of the kurtosis, particularly for the case of a symmetric distribution ($S_w \sim 0$ and/or $S_\theta \sim 0$), implies very small deviations from the rms average (as in a box-shaped distribution of probabilities with tails much smaller than the Gaussian distribution). A flow pattern which is divided into up- and downflows (or hot and cold areas) and which is characterized by a small kurtosis (and a skewness close to zero) can be viewed as representing a quasi-laminar state.

3.1 The quasi-normal approximation

Millionshchikov (1941) first suggested the hypothesis that for turbulent flows, FOMs of velocity and temperature could obey a Gaussian distribution. If the FOMs of fluctuations a, b, c and d around their mean values have a Gaussian distribution, then they can be expressed exactly in terms of SOMs:

$$\overline{abcd} = \overline{ab}\;\overline{cd} + \overline{ac}\;\overline{bd} + \overline{ad}\;\overline{bc}. \tag{10}$$

The quantities a, b, c and d follow a quasi-normal distribution, if equation (10) holds, but no further assumptions are made on them. Note that for an exact Gaussian (i.e. normal) distribution the TOMs would be zero. Only equation (10) was required to hold by Millionshchikov (1941). For the fluctuations of temperature, θ, and vertical velocity, w, this implies

$$\overline{w^4} = 3\overline{w^2}^2, \tag{11}$$

$$\overline{\theta^4} = 3\overline{\theta^2}^2, \tag{12}$$

$$\overline{w^3\theta} = 3\overline{w^2}\,\overline{w\theta}, \tag{13}$$

$$\overline{w\theta^3} = 3\overline{\theta^2}\,\overline{w\theta}, \tag{14}$$

$$\overline{w^2\theta^2} = \overline{w^2}\,\overline{\theta^2} + 2\overline{w\theta}^2. \tag{15}$$

For the case of shear driven turbulence, Frenkiel & Klebanoff (1967) measured higher order moments of velocities downstream of a grid and found even-order correlations of fourth (and sixth) order to be fairly well approximated by the assumptions of Gaussianity and isotropy for moments which involve only even powers ($\overline{w^4}$, $\overline{w^2u^2}$, $\overline{u^4}$, ...). All other moments measured by them were found to be poorly approximated using those assumptions. As convection is neither homogeneous (the background conditions are a function of location) nor isotropic, much larger deviations from (11)–(15) are to be expected. The quasi-normal approximation could still hold for the horizontal velocity components, i.e.

$$\overline{u^4} = 3\overline{u^2}^2, \tag{16}$$

$$\overline{v^4} = 3\overline{v^2}^2, \tag{17}$$

if horizontally the flow on average behaves as if it were isotropic.

One problem which occurs in non-local models of convection that assume equation (10), is that the TOMs can become excessively large. André et al. (1976a) hence suggested to limit the growth of the TOMs through clipping, i.e. to enforce the realizability constraints

$$\overline{abc}^2 \leqslant \min \begin{cases} \overline{a^2}\,(\overline{b^2c^2} - \overline{b^2}\;\overline{c^2}), \\ \overline{b^2}\,(\overline{a^2c^2} - \overline{a^2}\;\overline{c^2}), \\ \overline{c^2}\,(\overline{a^2b^2} - \overline{a^2}\;\overline{b^2}), \end{cases} \tag{18}$$

which can be obtained from applying the Cauchy–Schwartz inequality to algebraic relations between products of the TOMs (Blanchet 1970). The method was successfully applied in André et al. (1976b) to model the PBL of the earth. However, a convection model based on (11)–(15) with clipping of the TOMs may still not be able to match the data measured for a real flow. Gryanik et al. (2005) pointed out that the constraints

$$K_w \geqslant 1 + S_w^2 \quad \text{and} \quad K_\theta \geqslant 1 + S_\theta^2, \tag{19}$$

which can be derived from equation (18) by setting $a = b = c$ equal to w and θ, are fulfilled by their aircraft data and their numerical simulations, but could never be fulfilled, if equations (11) and (12) were to hold as well. The reason why equations (11) and (12) fail to fulfil equation (19) is that values for K_w and K_θ much larger than 3 occur in the data as well as values of S_w^2 and S_θ^2 larger than 2. However, equations (11) and (12) limit K_w and K_θ to 3 which cannot be realized in nature for values of $S_w^2 > 2$ and $S_\theta^2 > 2$, because this would violate equation (19). Such large values of S_θ^2 are nevertheless observed for convection in the atmosphere (Gryanik et al. 2005) and hence this deficiency of the quasi-normal approximation cannot be resolved by just clipping the TOMs. Fig. 2 demonstrates that similar conditions are also expected for convection in the Sun and other cool stars. For each layer in both the Sun and the K dwarf, the averaged K_w and S_w from the simulations are realizable solutions which fulfil equation (19). For the case of the Sun, quite a number of layers exist where $S_w^2 > 2$. Assuming equation (11) to hold is not consistent with realizable solutions for these layers. Fig. 3 confirms that similar results hold for K_θ and S_θ as well. Again the simulations easily fulfil equation (19). For both cases, more than half of the simulation domain includes layers where $S_\theta^2 > 2$ which is inconsistent with equation (12). Hence, a poor performance is expected for the quasi-normal approximation when applied to convection in the Sun and other cool stars. In Section 4, we investigate these results in more detail. We also note that for a fully compressible flow, such as stellar convection, the application of Favre averages would actually be required to strictly impose equations (18) and (19). However, even around the superadiabatic peak, where density fluctuations are largest, Favre-averaged SOMs of w and θ differ in our numerical simulations for the Sun from their plain average by less than 10 per cent. The most severe violations of equation (19) due to equations (11) and (12) occur in the quasi-adiabatic zone, where these differences drop from 4 per cent to less than 1 per cent near the bottom of the simulation box. Therefore, even in a Favre-averaged form, equation (19) would be violated by the quasi-normal approximation.

3.2 Eddy damping

Instead of resorting to clipping of lower order moments, Zeman & Lumley (1976) suggested to approximate FOMs which depend

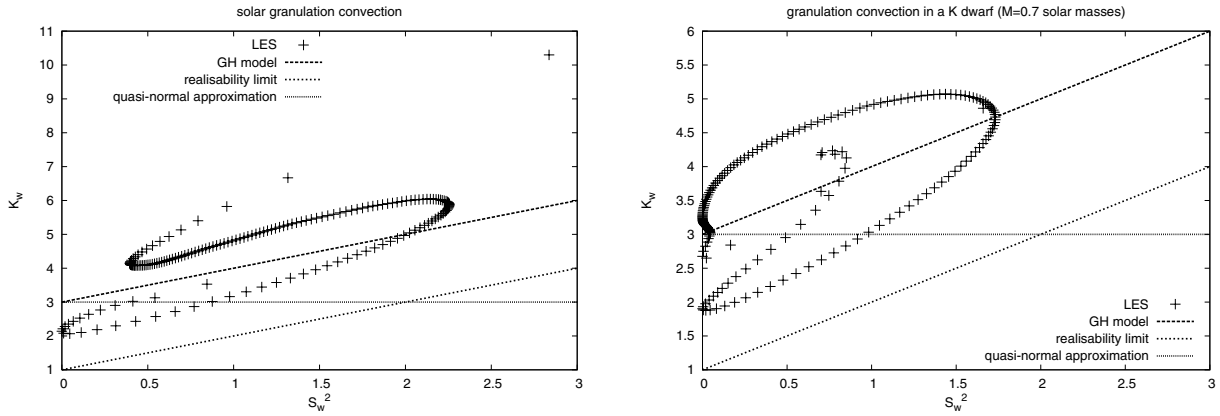

Figure 2. The left-hand panel demonstrates that our simulations (each layer is represented by a + sign) and the GH model (Section 3.3) fulfil the realizability conditions (19) of vertical velocity w for the case of the Sun. Note that for some layers (located mostly close to the centre of the simulation domain) $S_w^2 > 2$. The right-hand panel depicts the K dwarf case, where $S_w^2 < 2$ for all layers and conditions (19) hold as well.

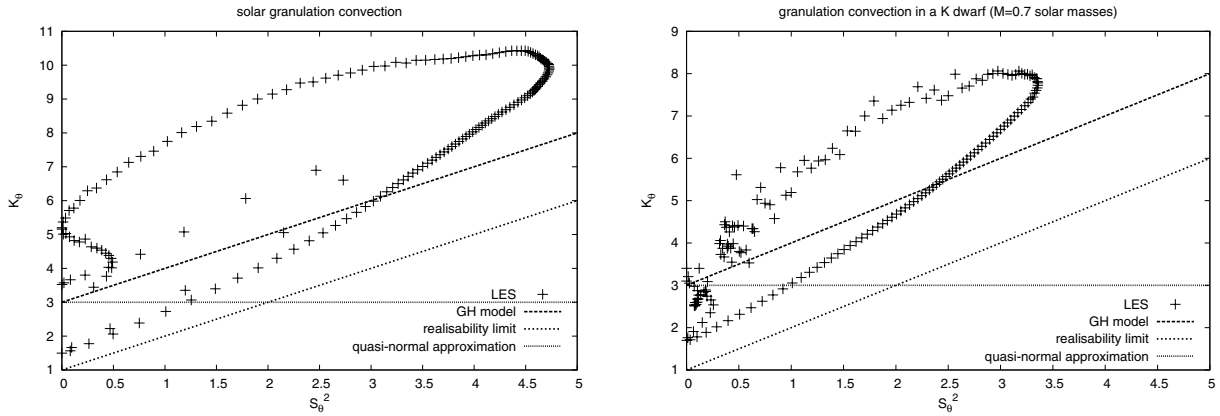

Figure 3. The left-hand panel shows that our simulations and the GH model (Section 3.3) fulfil the realizability conditions (19) of temperature θ for the case of the Sun (same notation as in Fig. 2). The right-hand panel depicts the K dwarf case, where conditions (19) also hold. For both cases and for many layers evidently $S_\theta^2 > 2$. The LES averages of $\overline{\theta^4}$ for the K dwarf are not yet converged for the two lowermost pressure scaleheights of the simulation domain, which explains the scatter in the upper branch of the LES data for K_θ (values from 8 down to 3.5), see also Figs 4 and 5.

only on velocity and temperature by the quasi-normal hypothesis (10) and FOMs which depend also on pressure by relaxation (i.e. damping) terms. It is thus not meaningful to reconstruct individual FOMs from such models, as they only aim at approximating the sum of all FOMs and their derivatives in each equation. Nevertheless, the eddy damping procedure is required to yield physically realizable solutions which approximate SOM and TOM of turbulent flows as closely as possible. This type of approach was first introduced by Hanjalić & Launder (1972) for the case of shear flows. It is the one-point average, real space equivalent of eddy damping, which was proposed by Orszag (1970) for turbulence models in Fourier space. Lumley, Zeman & Siess (1978) gave an overview on eddy-damped quasi-normal approximations and provided a physical interpretation of its ingredients for buoyancy driven turbulent transport. This approach was found to be at least as successful as the clipping of André et al. (1976a,b) for the prediction of non-local turbulent fluxes for the convective boundary layer of the earth as derived from field and laboratory experiments (Zeman & Lumley 1976; Lumley et al. 1978). Canuto (1992) generalized the approach of Zeman & Lumley (1976) by retaining dependences in the dynamical equations of the TOMs which had been discarded in earlier work to obtain a more manageable set of equations. On this basis, Canuto (1993) derived explicit relations for all TOMs in terms of SOMs. They were used in Canuto et al. (1994) for a non-local convection model for the PBL. In comparisons with numerical simulations, this new model was found to be more robust than its predecessor (Zeman & Lumley 1976). However, Zilitinkevich et al. (1999) pointed out that the model by Canuto et al. (1994), although quite satisfactory for $\overline{w^3}$ and $\overline{q^2 w}$, was less successful at reproducing the cross-correlation moments $\overline{w^2\theta}$ and $\overline{w\theta^2}$. This problem was resolved in Canuto, Cheng & Howard (2001) who suggested taking into account the degree of instability of the stratification within the convection zone when constructing the damping time-scale. With that improvement, the model was successfully applied to convection in A-stars (Kupka & Montgomery 2002) and white dwarfs (Montgomery & Kupka 2004). In this form, the model still does not directly account for the effects of coherent structures in convection zones on non-local transport. For a more detailed analysis of this class of models, we refer to Kupka (2007) and Kupka & Muthsam (2007). The main alternative to the eddy damping approach is to consider models which aim at directly improving the parametrization of the FOMs themselves.

3.3 The GH model

Mass-flux models have been used in atmospheric sciences since the pioneering work of Arakawa (1969) and Arakawa & Schubert (1974) on the interaction of convective cumulus clouds with their environment. Such models are based on the requirement that convective up- and downdrafts have to satisfy mass continuity, if their vertical exchange is averaged horizontally and integrated over sufficiently long time-scales. This is strictly imposed unless there is a net mass loss or gain at the boundaries. Randall, Shao & Moeng (1992) proposed a model for the convective boundary layer of the earth which represented a first step towards combining the concepts of mass-flux models and ensemble-averaged closure models. Subsequently, several closures for the dynamical equations of the SOMs were suggested which were based on mass-flux concepts. For example, Canuto & Dubovikov (1998) proposed a closure for $\overline{w^2\theta}$ and $\overline{w\theta^2}$ derived from mass-flux arguments while the other TOMs were required to be computed with the eddy-damped quasi-normal model of Canuto (1992, 1993). For $\overline{w^2\theta}$, the same model was proposed by Zilitinkevich et al. (1999) who also pointed out why mass-flux models are more appropriate than diffusion-type models to account for the non-local, coherently structured nature of boundary layer convection. In Mironov et al. (1999), the same authors show that to fulfil the symmetries of the TOMs with respect to sign changes of θ and w, it is necessary to modify the mass-flux models such that they separately account for the warm and cold fluid transported by the updrafts. Their model for $\overline{w^2\theta}$ and $\overline{w\theta^2}$ compared excellently with the measurements. However, no suggestions were provided how to compute S_w and S_θ which are required by the model as an input (in Mironov et al. 1999 they were taken from measurements).

The observational data from Gryanik & Hartmann (2002) confirmed earlier results for the convective PBL which claimed that the characteristic horizontal scales of θ are larger than those of w. The data also confirmed that $K_\theta \gtrsim K_w$ and $|S_\theta| \gtrsim |S_w|$. These results motivated Gryanik & Hartmann (2002) to develop the concepts proposed in Mironov et al. (1999) and describe the coherent structures within convective flows (e.g. downdrafts, granules or large plumes) by a two-scale mass-flux model. In this model, the different fractions of horizontal area which are covered by up- and downflows, a and $(1-a)$, as well as hot and cold drafts, b and $(1-b)$, are used to define a two-scale top-hat decomposition:

$$\langle v_z\rangle_{\rm mf} = a\, w_{\rm u} + (1-a)\, w_{\rm d}, \tag{20}$$

$$\langle T\rangle_{\rm mf} = b\,\theta_{\rm h} + (1-b)\,\theta_{\rm c}. \tag{21}$$

Here, $w_{\rm u}$ and $w_{\rm d}$ are the horizontal averages over *all* up- and downdrafts relative to the mean upwards velocity $\langle v_z\rangle_{\rm mf}$. Likewise, $\theta_{\rm h}$ and $\theta_{\rm c}$ are the horizontal averages over *all* areas hotter and colder than the mean temperature $\langle T\rangle_{\rm mf}$. For this *global* top-hat mass-flux average, all higher order moments can be given analytically as functions of a, b, $w_{\rm u}-w_{\rm d}$ and $\theta_{\rm h}-\theta_{\rm c}$. If instead one chooses as irreducible moments the quantities σ_w, σ_θ, $\langle w\theta\rangle_{\rm mf}$, S_w and S_θ, which here relate to the mass-flux average defined by equations (20) and (21), one can derive the following relations:

$$\langle w^2\theta\rangle_{\rm mf} = S_w\,\sigma_w\,\langle w\theta\rangle_{\rm mf}, \tag{22}$$

$$\langle w\theta^2\rangle_{\rm mf} = S_\theta\,\sigma_\theta\,\langle w\theta\rangle_{\rm mf}, \tag{23}$$

$$\langle w^4\rangle_{\rm mf} = \left(1+S_w^2\right)\sigma_w^4, \tag{24}$$

$$\langle \theta^4\rangle_{\rm mf} = \left(1+S_\theta^2\right)\sigma_\theta^4, \tag{25}$$

$$\langle w^3\theta\rangle_{\rm mf} = \left(1+S_w^2\right)\sigma_w^2\,\langle w\theta\rangle_{\rm mf}, \tag{26}$$

$$\langle w\theta^3\rangle_{\rm mf} = \left(1+S_\theta^2\right)\sigma_\theta^2\,\langle w\theta\rangle_{\rm mf}. \tag{27}$$

They are exact only if fluctuations within and among the drafts can be neglected (global top-hat average).

In Gryanik et al. (2005), an alternative interpretation of the model was given which can be generalized more easily. Consider the realizations of w and θ in a flow. The two-scale mass-flux model is obtained, if one approximates the joint probability density function of w and θ as the sum of four δ-functions. Each of them represents one out of four possibilities for a given pair (w,θ) to be in an up- or downdraft which is either hotter or colder than the average. Through integration over all pairs (w,θ) of a given realization (e.g. a set of measurements) the probability for each of the four possibilities is obtained and mean values for the drafts $(w_{\rm u},\ldots)$ are assigned (Gryanik & Hartmann 2002 required an additional symmetry to hold which is dropped in this new interpretation). Neglecting fluctuations within and among the drafts requires approximating the actual probability density function of (vertical) velocity and temperature fluctuations with δ-functions. In the limit of large $|S_w|$ and $|S_\theta|$, one type of draft (up or down, hot or cold) becomes very localized and dominates the statistics (Gryanik & Hartmann 2002), for which the 4δ probability density function becomes an increasingly better approximation. In that case, the averages (22)–(27) should approximate the ensemble average. Hence, Gryanik & Hartmann (2002) and Gryanik et al. (2005) suggested to take

$$\overline{w^2\theta} = S_w\,\sigma_w\,\overline{w\theta} = \left(\overline{w^3}/\overline{w^2}\right)\,\overline{w\theta}, \tag{28}$$

$$\overline{w\theta^2} = S_\theta\,\sigma_\theta\,\overline{w\theta} = \left(\overline{\theta^3}/\overline{\theta^2}\right)\,\overline{w\theta}, \tag{29}$$

$$\overline{w^4} = S_w^2\,\overline{w^2}^2, \tag{30}$$

$$\overline{\theta^4} = S_\theta^2\,\overline{\theta^2}^2, \tag{31}$$

$$\overline{w^3\theta} = S_w^2\,\overline{w^2}\,\overline{w\theta}, \tag{32}$$

$$\overline{w\theta^3} = S_\theta^2\,\overline{\theta^2}\,\overline{w\theta}, \tag{33}$$

$$\overline{w^2\theta^2} = S_w\,S_\theta\,\overline{w\theta}\,\sigma_w\,\sigma_\theta, \tag{34}$$

in the limit of large $|S_w|$ and $|S_\theta|$. We note that here and in the following, S_w, S_θ, σ_w and σ_θ are again computed from ensemble averages, equations (7) and (8), a step which is motivated further below. Equation (34) was given only in Gryanik et al. (2005), who actually considered a more general case in which a flow can also have a large skewness for its horizontal velocities. That model is based on a 16δ probability density function.

Mass-flux models, such as (20)–(27), do not account for fluctuations within the coherent structures of the flow or among them. It is possible to extend equation (20) to account for *subplume* and *interplume* fluctuations by performing an exact splitting into the different contributions (see Siebesma & Cuijpers 1995 and Petersen et al. 1999 – note that in astrophysics the term plume is also applied to subplume structures within a downdraft). The same kind of splitting can naturally be done for equation (21). However, to become predictive rather than just diagnostic, such models have to be tailored to a specific application, because they require a detailed understanding and modelling of the behaviour of the turbulent flow within the up- and downdrafts. For the quasi-adiabatic layers in the solar convection zone, such a model is proposed in Belkacem et al.

(2006a) based on the exact splitting of the different contributions from fluctuations within and among drafts to a given moment and a plume model.

The fact that both coherent structures and fluctuations within them contribute to the statistics of the flow is also evident from the data discussed in Gryanik & Hartmann (2002). At the same time, as they show in their fig. 7, there is a remarkably linear correlation between two-scale mass-flux averages and Reynolds averages for $\overline{w^2}$, $\overline{w\theta}$ and $\overline{\theta^2}$. It even holds with a larger scatter for $\overline{w^3}$ and $\overline{\theta^3}$ (and also for the remaining quantities displayed, $\overline{w^2\theta}$, $\overline{w\theta^2}$, $\overline{w^4}$ and $\overline{\theta^4}$). On the strength of this result, they suggested that the two-scale mass-flux averages can be replaced by Reynolds averages, if linear scaling factors are introduced. Specifically, for the FOMs in equations (30)–(34),

$$\overline{w^4} = a_3 \left(1 + d_3 S_w^2\right) \overline{w^2}^2, \tag{35}$$

$$\overline{\theta^4} = a_4 \left(1 + d_4 S_\theta^2\right) \overline{\theta^2}^2, \tag{36}$$

$$\begin{aligned} \overline{w^3\theta} &= a_5 \left(1 + d_5 S_w^2\right) \overline{w^2}\,\overline{w\theta} \\ &= a_5 \left(1 + d_5 S_w^2\right) C_{w\theta}\, \sigma_w^3\, \sigma_\theta, \end{aligned} \tag{37}$$

$$\begin{aligned} \overline{w\theta^3} &= a_6 \left(1 + d_6 S_\theta^2\right) \overline{\theta^2}\,\overline{w\theta} \\ &= a_6 \left(1 + d_6 S_\theta^2\right) C_{w\theta}\, \sigma_w\, \sigma_\theta^3, \end{aligned} \tag{38}$$

$$\begin{aligned} \overline{w^2\theta^2} &= a_7 \left[(\overline{w^2}\,\overline{\theta^2} + 2\overline{w\theta}^2) + d_7 S_w\, S_\theta\, \overline{w\theta}\, \sigma_w\, \sigma_\theta\right] \\ &= a_7 \left(1 + d_7 \frac{C_{w\theta}}{1 + 2\,C_{w\theta}^2} S_w\, S_\theta\right) \left(1 + 2\,C_{w\theta}^2\right)\, \sigma_w^2\, \sigma_\theta^2 \end{aligned} \tag{39}$$

(Gryanik & Hartmann 2002; Gryanik et al. 2005). The quantities $a_i (i = 3, \ldots, 7)$ and $d_i (i = 3, \ldots, 7)$ are dimensionless parameters. Similar relations can be derived for the horizontal components of the velocity fluctuations (Gryanik et al. 2005). To complete their model for FOMs, Gryanik & Hartmann (2002) and Gryanik et al. (2005) required that for zero skewness equations (35)–(39) reproduce the quasi-normal limit (equations 11–15). This is possible, provided

$$a_i = 3 \quad (i = 3, \ldots, 6), \quad a_7 = 1. \tag{40}$$

If at the same time for large $|S_w|$ and $|S_\theta|$ relations (35)–(39) should match equations (30)–(34), one has to choose

$$d_i = \frac{1}{3} \quad (i = 3, \ldots, 6), \quad d_7 = 1. \tag{41}$$

Hence, the choice of the d_i is motivated both by the linear correlation observed between the Reynolds and the mass-flux averages, and by the notion that they should coincide if one type of draft becomes very localized. Model (equations 35–41) identifies coherent structures as the main cause of deviations from an otherwise quasi-normal distribution of FOMs. However, instead of just being an ad hoc expansion around the quasi-normal approximation, its specific form is suggested by the flow structure and linear correlations found in the data. Naturally, the model (equations 35–41) can only be considered an approximation to the statistics of real convective flows, because zero skewness does not imply a Gaussian distribution (K_w and K_θ may be both larger and smaller than 3) and contributions from fluctuations within the up- and downdrafts may be significant even for large values of $|S_w|$ and $|S_\theta|$. Both the coherent structure of up- and downdrafts and more local phenomena such as fluctuations within a downdraft, contribute to S_w and S_θ. Consequently, tests through measurements and simulations are required to determine the range over which the model can accurately predict FOMs.

Gryanik & Hartmann (2002) also studied possible benefits from individual optimizations of the corresponding a_i and d_i for equations (35)–(38) by applying least-square minimization to their measurements. Improvements due to individual tuning of the a_i and d_i were found to be negligible for $\overline{w^4}$ as well as $\overline{\theta^4}$ (at most 1 per cent as measured by the explained variance) and small for $\overline{w^3\theta}$ as well as $\overline{w\theta^3}$ (no more than 10 per cent in terms of explained variance). No systematic offsets or trends were observed for equations (40) and (41) or for the optimized choices of a_i and d_i.

For that reason, we restrict our comparisons in Section 4 to

$$\overline{w^4} = 3\left(1 + \frac{1}{3} S_w^2\right) \overline{w^2}^2, \tag{42}$$

$$\overline{\theta^4} = 3\left(1 + \frac{1}{3} S_\theta^2\right) \overline{\theta^2}^2, \tag{43}$$

$$\overline{w^3\theta} = 3\left(1 + \frac{1}{3} S_w^2\right) \overline{w^2}\,\overline{w\theta}, \tag{44}$$

$$\overline{w\theta^3} = 3\left(1 + \frac{1}{3} S_\theta^2\right) \overline{\theta^2}\,\overline{w\theta}, \tag{45}$$

$$\overline{w^2\theta^2} = \overline{w^2}\,\overline{\theta^2} + 2\overline{w\theta}^2 + S_w\, S_\theta\, \overline{w\theta}\, \sigma_w\, \sigma_\theta, \tag{46}$$

which we refer to as the GH model. To illustrate the lack of benefits from optimizing the coefficients in these relations and for the much greater importance of maintaining the correct functional form of the approximations, we investigate two models proposed by Grossman & Narayan (1993). They share formal similarities with equations (35)–(39).

3.4 Expansions in powers of TOMs

Grossman & Narayan (1993) used smoothed particle hydrodynamics (SPH) simulations to study convection in a box for idealized microphysics and idealized boundary conditions. They used their simulations to test a number of closure relations for higher order moments. For the case of FOMs, they also suggested to account in an (ad hoc) manner for the asymmetries in the instantaneous distributions of velocity and temperature fluctuations which were evident in their SPH convection simulations. They proposed to consider lowest-order expansions in terms of S_w or all the TOMs, respectively, around the expressions of the quasi-normal hypothesis (equations 11–15).

The first model of Grossman & Narayan (1993) we are interested in here is their Model 3 for FOMs (equations 42a–42e in Grossman & Narayan 1993, with the numerical parameters $\eta = 2.3$ and $\zeta = 1.8$ taken from their table 11):

$$\overline{w^4} = \left(2.3 + 1.8 S_w^2\right) \overline{w^2}^2, \tag{47}$$

$$\overline{\theta^4} = \left(2.3 + 1.8 S_w^2\right) \overline{\theta^2}^2, \tag{48}$$

$$\overline{w^3\theta} = \left(2.3 + 1.8 S_w^2\right) \overline{w^2}\,\overline{w\theta}, \tag{49}$$

$$\overline{w\theta^3} = \left(2.3 + 1.8 S_w^2\right) \overline{\theta^2}\,\overline{w\theta}, \tag{50}$$

$$\overline{w^2\theta^2} = \left(2.3 + 1.8S_w^2\right)\left(\frac{1}{3}\overline{w^2}\,\overline{\theta^2} + \frac{2}{3}\overline{w\theta}^2\right). \quad (51)$$

In the following, we refer to equations (47)–(51) as model GN3.

The second suggestion we are interested in is their Model 4 for FOMs (equations 43a–43e in Grossman & Narayan 1993 with $\eta = 2.3$ and $\zeta = 2.1$ from their table 11):

$$\overline{w^4} = \left(2.3 + 2.1S_w^2\right)\overline{w^2}^2, \quad (52)$$

$$\overline{\theta^4} = \left(2.3 + 2.1S_\theta^2\right)\overline{\theta^2}^2, \quad (53)$$

$$\overline{w^3\theta} = \left(2.3 + 2.1\frac{\overline{w^2\theta}^2}{\sigma_w^4\,\sigma_\theta^2}\right)\overline{w^2}\,\overline{w\theta}, \quad (54)$$

$$\overline{w\theta^3} = \left(2.3 + 2.1\frac{\overline{w\theta^2}^2}{\sigma_w^2\,\sigma_\theta^4}\right)\overline{\theta^2}\,\overline{w\theta}, \quad (55)$$

$$\overline{w^2\theta^2} = \left(2.3 + 2.1\frac{\overline{w^2\theta}^2}{\sigma_w^4\,\sigma_\theta^2}\right)\frac{1}{3}\overline{w^2}\,\overline{\theta^2} + \left(2.3 + 2.1\frac{\overline{w\theta^2}^2}{\sigma_w^2\,\sigma_\theta^4}\right)\frac{2}{3}\overline{w\theta}^2. \quad (56)$$

We refer to equations (52)–(56) as model GN4.

Comparing the model of Gryanik & Hartmann (2002) and Gryanik et al. (2005) with the suggestions by Grossman & Narayan (1993), we note that equations (35), (36) and (37) given above correspond to equations (42a), (43e) and (42b) of Grossman & Narayan (1993), respectively, see equations (47), (53) and (49) given above, if $a_3 = a_4 = a_5 = \zeta$ and $d_3 = d_4 = d_5 = \eta/\zeta$, where η and ζ are the numerical constants used in models GN3 and GN4. However, equations (38) and (39) have no counterpart among any of their suggestions. Various SPH simulations were used by Grossman & Narayan (1993) to find the best-fitting values $\eta \approx 1.8, \ldots, 2.1$ as well as $\zeta \approx 2.3$ by simultaneous fits for the expressions suggested for each of $\overline{w^4}$, $\overline{w^3\theta}$, $\overline{w^2\theta^2}$, $\overline{w\theta^3}$ and $\overline{\theta^4}$. Compared to Gryanik & Hartmann (2002) and Gryanik et al. (2005), no further physical justification was provided in Grossman & Narayan (1993) for the particular form of equations (47)–(56) other than that of plausible symmetries (but see also Section 4.1).

As we noted in Section 3.3, Gryanik & Hartmann (2002) and Gryanik et al. (2005) found that individual 'tuning' of the coefficients a_i and d_i in (35)–(39) yields only small improvements over equations (40) and (41) for the PBL of the earth. We show in Section 4 that GN3 and GN4 are usually either comparable or less satisfactory than the GH model (equations 42–46).

4 RESULTS

4.1 Basic properties and horizontal flow

Figs 2 and 3 show that our numerical simulations fulfil the realizability conditions (19) for both vertical velocity and temperature. We note that the quasi-normal approximation as well as the GH and GN4 models and for most aspects also the GN3 model each fulfil all constraints posed by dimensional analysis, tensor invariance and symmetry conditions.[1] Moreover, they are reversible in time, i.e. the moments remain the same under the transformation $t \to -t$. With (40)–(41) equations (35)–(39) also fulfil various realizability requirements. In particular, the GH model equations for $\overline{w^4}$ and $\overline{\theta^4}$, (42) and (43), fulfil (19) for all possible values of S_w and S_θ, as can immediately be seen from Figs 2 and 3 and by trivial algebra. We also note that equations (24) and (25) of the two-scale mass-flux model of Gryanik & Hartmann (2002) exactly define the lower boundary for K_w and K_θ for any model that is realizable for all values of S_w and S_θ. The GN4 model equations for $\overline{w^4}$ and $\overline{\theta^4}$, equations (52) and (53), share these properties of fulfilling equation (19) for all S_w and S_θ. The same holds for the GN3 model equation (47) for $\overline{w^4}$. However, in general this is not the case for equation (48), the GN3 model equation for $\overline{\theta^4}$, because it is not always true that $S_w^2 \geqslant S_\theta^2$. Figs 2 and 3 show that in fact for both simulations, S_θ^2 spans a much larger range than S_w^2. Inspection of both S_w and S_θ in Fig. 5 confirms that for both the solar granulation simulation and the granulation simulation for the K dwarf, the realizability constraint for θ in equation (19) is violated by equation (48) for some of the deeper layers, within the quasi-adiabatic part of the convection zone. For equations (11) and (12) of the quasi-normal model the violation of the realizability constraints, equation (19) has already been pointed out in Section 3.1. This is a result of the large values for S_w and S_θ found for the case of vertical velocities in the solar granulation simulation and for the case of temperature fluctuations for both the solar and the K dwarf simulations, as can easily be seen in Figs 2 and 3. As they fail to match realizability conditions, we expect the GN3 model and the quasi-normal approximation to perform poorly, if used to model fluctuations in vertical velocities and temperature in solar surface convection and surface convection in cool stars. On the other hand, the GH model and the GN4 model always provide realizable solutions.

Before considering a detailed comparison of these models, we will describe some aspects of kurtosis and skewness found for the solar and the K dwarf simulations. Fig. 4 shows the kurtoses K_w and K_θ for each case. Apart from a few separated layers, there is no particular region in which the quasi-normal value of 3 is attained. The surface layers ($\ln P \lesssim 11.7$ for the solar case and $\lesssim 12.3$ for the K dwarf one) show a complex behaviour. Near the superadiabatic peak (around $\ln P \sim 12$ and 13, respectively), the kurtosis becomes as small as 2, even 1.5 in the case of K_θ for the solar simulation. In the underlying quasi-adiabatic zone, the kurtoses become much larger: reaching between 5 and 6 for K_w, and between 8 and 10 for K_θ. These large values are a consequence of the large velocity and temperature fluctuations which are related to the narrow, cold downdrafts and the constraint of mass conservation (see the discussion of S_w and S_θ given below). The behaviour in the lowermost two pressure scaleheights is less interesting, as it is the result of the closed lower boundary of the simulation domain. Evidently, the quasi-normal approximation can merely give order of magnitude estimates for the kurtoses (and hence for $\overline{w^4}$ and $\overline{\theta^4}$). Improvements over the quasi-normal approximation require a boost in the quasi-adiabatic region which can be provided by the GH model, the GN3 and the GN4 models. Values smaller than 2, as required in the superadiabatic layers, cannot be obtained from any of these models. Hence results in the vicinity of the superadiabatic peak will be much less satisfactory.

[1] Note that model GN3 does have some limitations with respect to symmetries. Although left- and right-hand sides remain self-consistent, if $w \to -w$ and/or $\theta \to -\theta$, division of (48) by σ_θ^4 yields $K_\theta = (2.3 + 1.8\,S_w^2)$ which is possible only if $w = c\theta$ where c is a dimensional constant. The latter is unlikely to hold for any non-trivial flow field.

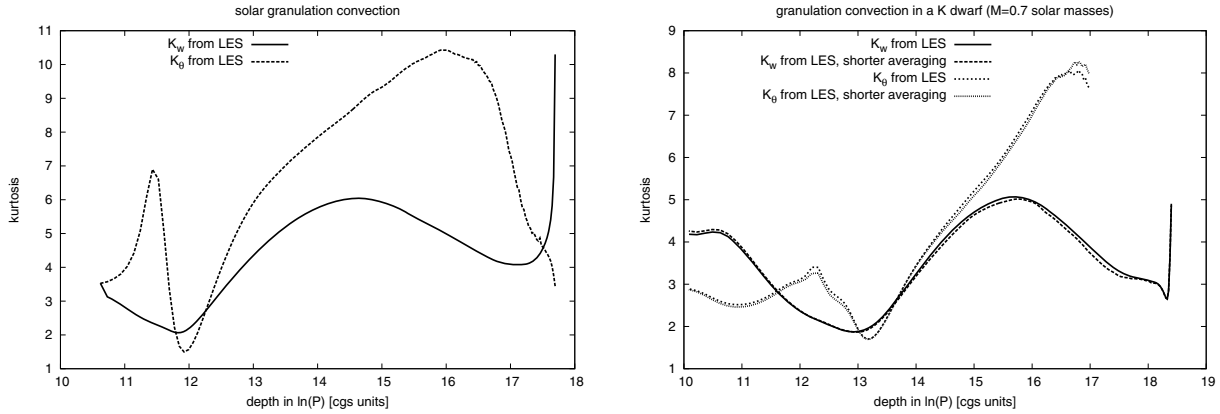

Figure 4. The left-hand panel shows the kurtosis of vertical velocity, K_w, and of temperature, K_θ, for the case of the Sun. Both are well converged. K_w is well converged for the case of the K dwarf, too. This is demonstrated in the right-hand panel by a comparison of an average taken over the first third of the total integration time with the average over the entire integration time. For K_θ, the same holds down to $\ln P \sim 16.5$, where in addition to differences between the two averages also oscillations begin to appear. Below $\ln P \sim 17$, these attain up to $\sim$25 per cent preventing interpretation of K_θ for $\ln P > 17$. The data for that bottom range are shown in Fig. 3.

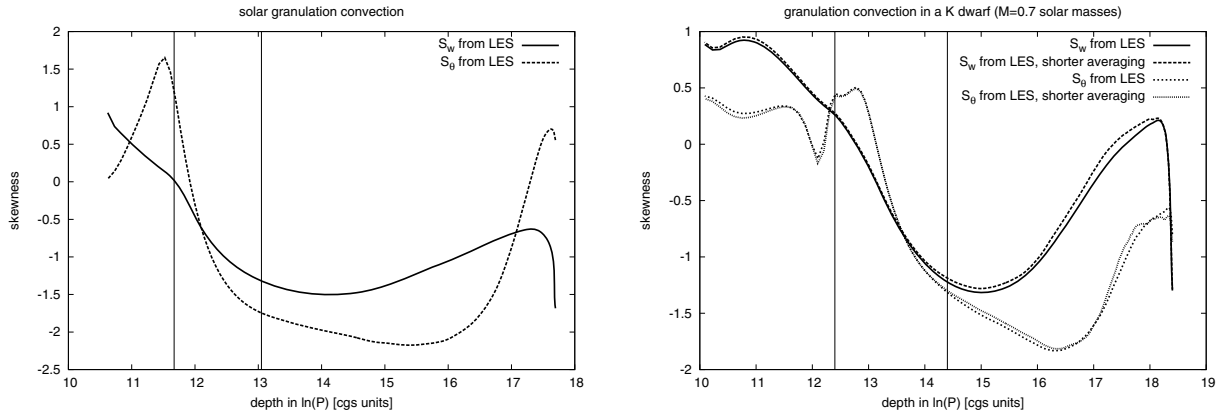

Figure 5. The left-hand panel shows the skewness of vertical velocity, S_w, and of temperature, S_θ, for the case of the Sun. Both are well converged. The same holds for S_w for the K dwarf case. This is shown in the right-hand panel, where an average taken over the first third of the total integration time is compared with the average over the entire integration time. S_θ appears well converged, too, as the small oscillations present in the shorter averaging have disappeared after longer averaging. For both cases, we also indicate the upper ($\nabla - \nabla_{\rm ad} = 0$, Z_1 from Table 1) and lower ($\nabla - \nabla_{\rm ad} \sim 0.03$, Z_2 from Table 1) boundaries of the superadiabatic layer through vertical lines.

Fig. 5 shows the skewnesses S_w and S_θ for the solar and the K dwarf case. It also indicates the upper and lower boundaries of the superadiabatic layer, outside of which $\nabla - \nabla_{\rm ad} < 0$ and $0 < \nabla - \nabla_{\rm ad} \lesssim 0.03$ hold, respectively (as defined in Table 1 and Section 1). Note that for both cases, both S_w and S_θ are positive in the photospheric (surface) layers. They also change sign roughly at the same location, around the superadiabatic peak (for the K dwarf this behaviour is more complex).

Large negative values occur within the quasi-adiabatic region for both functions in both stars. In particular, the absolute values of S_θ are large enough for the quasi-normal approximation to yield non-realizable results. The dominant contribution to the large values of K_w and K_θ found in the same layers can thus be assigned to the asymmetry of the flow which is also responsible for the large values of S_w^2 and S_θ^2. Thus, a significant 'boost' of $\overline{w^4}$ and other FOMs can be expected from the GH (and also the GN3 and GN4) model for these layers. For layers with $\ln P > 14$ in the Sun and $\ln P > 15$ in the K dwarf, there is also an important contribution from fluctuations within and among the drafts. The behaviour of the two lowermost pressure scaleheights is again strongly influenced by the lower boundary and of little interest in a stellar context. Throughout most of the simulation domain, the deviation from zero skewness is found to be large for both types of stars which is to be expected for an inhomogeneous flow. The superadiabatic region is the only region in which $S_w \sim 0$ and $S_\theta \sim 0$ at similar locations for the Sun and the K dwarf.

We recall that in the same region, the minimum values for K_w and K_θ are found. Moreover, $\overline{\theta^2}$ and $\overline{\theta^4}$ have their maxima right there. In the following, we give a physical explanation for these low values of K_w and K_θ. Within the superadiabatic region fluid ascending from below begins to cool rapidly. Fluid hotter than average is subject to even further enhanced cooling. The same happens to fluid travelling through this zone faster than average. Each of these processes is smoothing out vertical velocity and temperature fluctuations about the mean within the updraft. Moreover, as a consequence of cooling the buoyancy experienced by the ascending fluid is reduced. Material cooling faster than average is hence being dragged downwards, if located near the boundary of an upflow, or reheated rapidly by its environment. The net result is a *quasi-laminar* appearing upflow (cf. Stein & Nordlund 1998). Thus, even if there are still

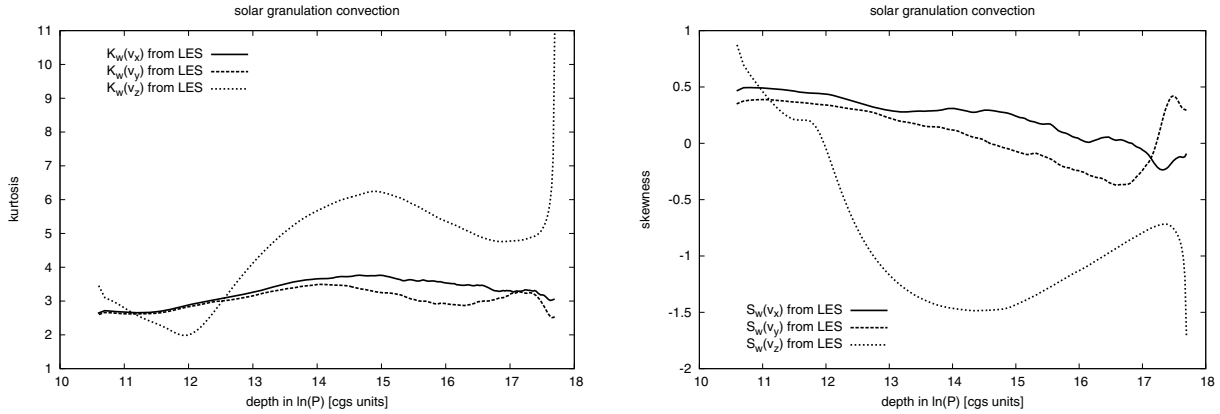

Figure 6. The left-hand panel shows the kurtosis of horizontal (x and y) and vertical (z) velocity components for the case of the Sun. The right-hand panel shows the skewness of the different velocity components in the same run. The oscillations still present in the x and y components for the lower half of the simulation domain in both K_w and S_w imply that further averaging would be required for a more detailed interpretation.

fluctuations in the downdrafts, the horizontally averaged K_w and K_θ can become significantly less than 3. This decrease is less pronounced for the K dwarf which has a shallower superadiabatic peak. Interestingly, this phenomenon is not limited to simulations with realistic microphysics. Inspection of fig. 11 in Chan & Sofia (1996) reveals that the same occurs in their simulation for a deep atmosphere with idealized microphysics (perfect gas equation of state, prescribed conductivity, radiative transfer in diffusion approximation).[2] The same general nature cannot be corroborated for the large values of K_θ in the photosphere. We found them only for the solar case which points to differences in the detailed mechanisms of cooling and reheating in the photosphere when compared to the simulation for the K dwarf. The solar values of $K_\theta \sim 7$ in the photosphere around $\ln P \sim 11.5$ are too large to be explained by $S_\theta^2 \sim 2.7$ and thus flow asymmetry. There has to be a substantial contribution from intermittent events such as splitting of existing and formation of new granules (cf. again Stein & Nordlund 1998).

A similar result is not found for the horizontal velocity field. Fig. 6 compares the kurtosis of the vertical velocity component $K_w = K_w(v_z)$ with that one of both horizontal components, $K_w(v_x)$ and $K_w(v_y)$, for the solar simulation. Both horizontal components yield quite similar results with values around 3 to within $\sim$25 per cent. Evidently, the quasi-normal approximation yields a reasonable estimate for the kurtosis of horizontal flow in all layers.

Whether the trend of values <3 in the surface layers and >3 in the layers underneath is realistic cannot be concluded from the present simulations because of the limited accuracy of the averages. This is evident from the remaining differences between x and y components. For a horizontally large enough simulation box and a sufficiently long run they should be identical, because the physical situation is symmetric in x and y components. As discussed in Robinson et al. (2003), the horizontal velocity averages and moments are some of the most difficult quantities to converge. The main reason for that problem is the overall increase of scales of the flow structures with depth while in turn small-scale fluctuations advected upwards through the stratification are smoothed out. The better convergence of averages of vertical velocities and temperatures compared to horizontal ones is also clear from the absence of small wiggles when comparing Figs 4–6 for values of $\ln P$ between 14 and 15.

The 'quasi-normal picture' for the horizontal flow components is underlined by the skewnesses of velocity which are also shown in Fig. 6. For both v_x and v_y, the absolute value of the skewness remains less than $1/2$. We expect the trend with positive values in the upper layers and negative ones near the bottom to be caused by the limitations in domain size and averaging time, similar to the kurtoses discussed above. Thus, a significantly longer averaging time should provide further evidence for an *approximately* quasi-normal behaviour of horizontal velocities, even though complex horizontal flow patterns are visible in individual snapshots of the velocity field such as Fig. 1.

4.2 Fourth-order moments

We now compare $\overline{w^4}$, $\overline{w^3\theta}$, $\overline{w^2\theta^2}$, $\overline{w\theta^3}$ and $\overline{\theta^4}$ computed directly from the numerical simulations, with the predictions of the different models introduced in Section 3. We present a consistency test which requires the computation of the right-hand side of the model equations (involving SOMs and TOMs) using the simulation data as their input. Figs 7–11 show the ratio of the values for FOMs obtained from a direct ensemble average of the simulation data to the values obtained when simulation data are used to evaluate the right-hand side of the model equations (11)–(15), (42)–(46), (47)–(51) and (52)–(56). Ideally, this ratio should be close to 1, within the uncertainties introduced by the simulations themselves. However, such uncertainties cannot explain the large deviations found for the ratio of $\overline{w^4}$ to its quasi-normal approximation (see Fig. 7). An overestimation (ratio less than 1) for the surface and superadiabatic layers is followed by an underestimation in the quasi-adiabatic zone (we again neglect here and in the following the lowermost two pressure scaleheights). Deviations range from a factor of up to 2 in the solar case to about 1.7 for the K dwarf. The other three models do a much better job than the quasi-normal approximation in modelling the quasi-adiabatic zone: the discrepancies are reduced to a factor of 1.2 for the GH model and also for GN3 and GN4 models. For the surface layers, the improvements are comparable, but the larger discrepancies found for the quasi-normal approximation

[2] The coincidence of minima of K_w and K_θ with $S_w \sim 0$ and $S_\theta \sim 0$ and with maxima of $\overline{\theta^2}$ and $\overline{\theta^4}$ as well as with the location of the superadiabatic peak can be verified, too. Figs 2 and 7 of Chan & Sofia (1996) confirm the properties of S_w, S_θ and $\overline{\theta^2}$. For a closely related simulation run made available to us by K. L. Chan, the complete set of properties could be confirmed.

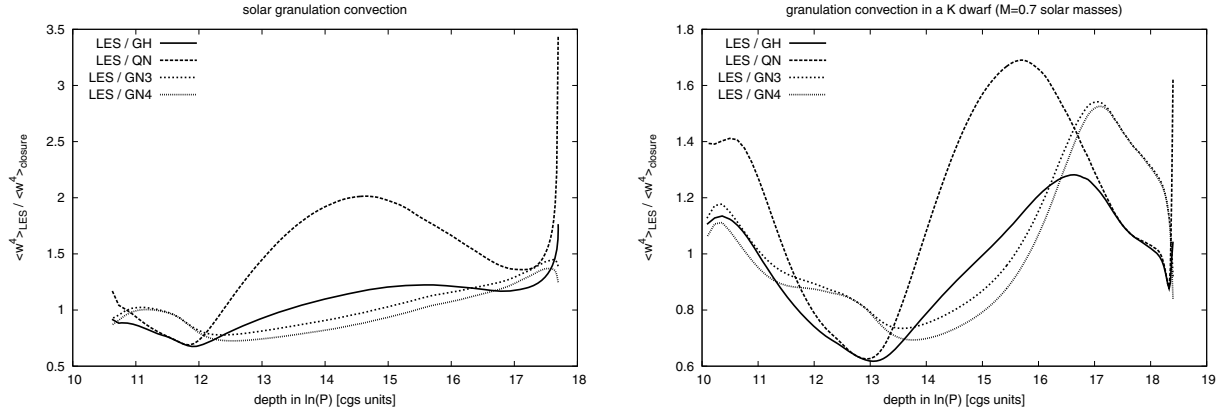

Figure 7. The ratios of $\overline{w^4}$ computed from LES to different closures evaluated using the LES are shown for the case of the Sun (left-hand panel) and the K dwarf (right-hand panel). Ensemble (Reynolds) averages are shown here and in Figs 8–13 and are explained in the text.

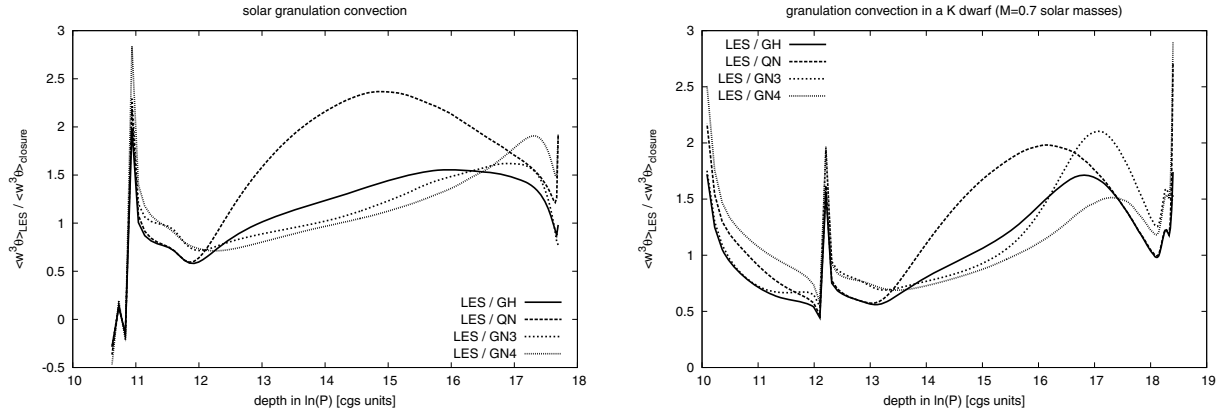

Figure 8. The ratios of $\overline{w^3\theta}$ computed from LES to different closures evaluated using the LES are shown for the case of the Sun (left-hand panel) and the K dwarf (right-hand panel).

remain unaltered for these models in the superadiabatic zone. This is expected from the results on K_w and S_w discussed in Section 4.1.

Similar results are found for $\overline{w^3\theta}$ as shown in Fig. 8. Compared to $\overline{w^4}$ the quasi-normal approximation expression (13) for $\overline{w^3\theta}$ performs even worse in the quasi-adiabatic part of the convection zone, where it underestimates the absolute value of the direct average by up to a factor of 2.3 in the solar case and 2.0 for the K dwarf simulation. Again the GH, GN3 and GN4 models provide improvements, although underestimations are larger compared to the case of $\overline{w^4}$ (up to a factor of 1.5 which is attained in the bottom part of the simulation domain, but is probably influenced by the lower boundary conditions). The GN4 model provides slightly better results than the GH model in the quasi-adiabatic part of the convection zone. However, its deviations are the largest ones in the photosphere where $\overline{w^3\theta}$ changes sign (around $\ln P \sim 11$ and $\sim$12.1 for the Sun and the K dwarf, respectively; the negative sign of the ratio which occurs for the top layers indicates that the correct location of the double change of sign of this quantity is very sensitive to the modelling, although it is likely that it depends on the choice of the boundary conditions as well). As for $\overline{w^4}$, none of the models is satisfactory in the region around the superadiabatic peak. The improvements obtained with the GN3 and GN4 models (overestimation of $|\overline{w^3\theta}|$ by less than a factor of 1.4) compared to the GH model is traded against larger deviations in the quasi-adiabatic zone (GN3 model) and the photosphere (GN4 model). Among the five FOMs, this one clearly is the most difficult to model.

In the case of $\overline{w^2\theta^2}$, the quasi-normal approximation again performs far worse than any of the other models tested here, with deviations of up to a factor of 2.6 in the solar and 2.3 in the K dwarf case, as shown by Fig. 9. The GH model provides significant improvements for the quasi-adiabatic region with deviations less than a factor of 1.5 for both cases (neglecting again the layers closer to the bottom than two pressure scaleheights). In the photospheric layers, the model behaves similarly to the quasi-normal approximation. The GN3 model is clearly further off than the GH model, notably in the quasi-adiabatic region, although this may also be influenced by the lower boundary. The GN4 model overall is slightly better, apart from the photosphere where it is worst among the models compared here.

For the case of $\overline{w\theta^3}$, the differences between the four models are most pronounced. Fig. 10 clearly shows that the quasi-normal approximation yields unacceptable results with deviations exceeding a factor of 3 for the solar case and 2.5 for the K dwarf. This is in a region located more than two pressure scaleheights above the lower boundary. Deviations are also large near the superadiabatic peak (factor of 2 too small). The GH model is clearly the most successful one in recovering this quantity. Deviations remain less than a factor of 1.3 throughout most of the quasi-adiabatic region for both the solar and the K dwarf case (i.e. between the levels Z_2 and Z_3 defined

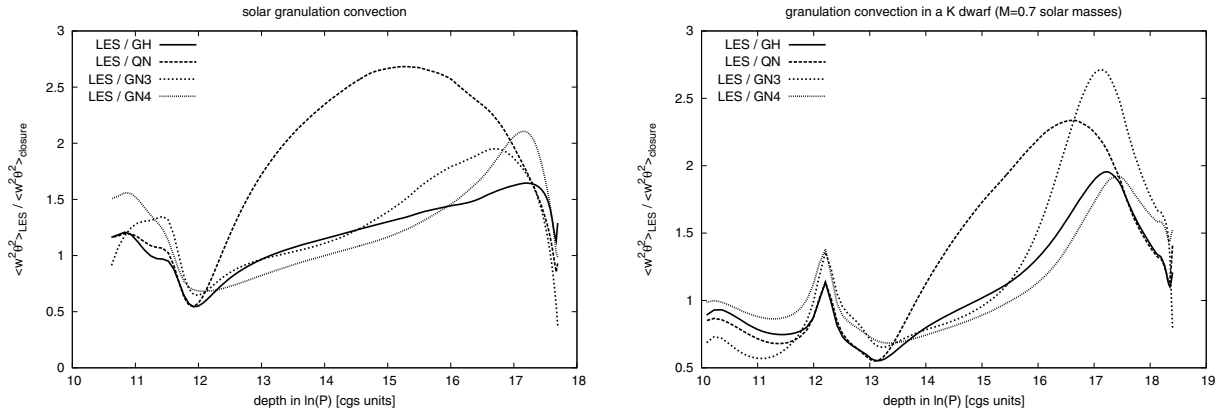

Figure 9. The ratios of $\overline{w^2\theta^2}$ computed from LES to different closures evaluated using the LES are shown for the case of the Sun (left-hand panel) and the K dwarf (right-hand panel).

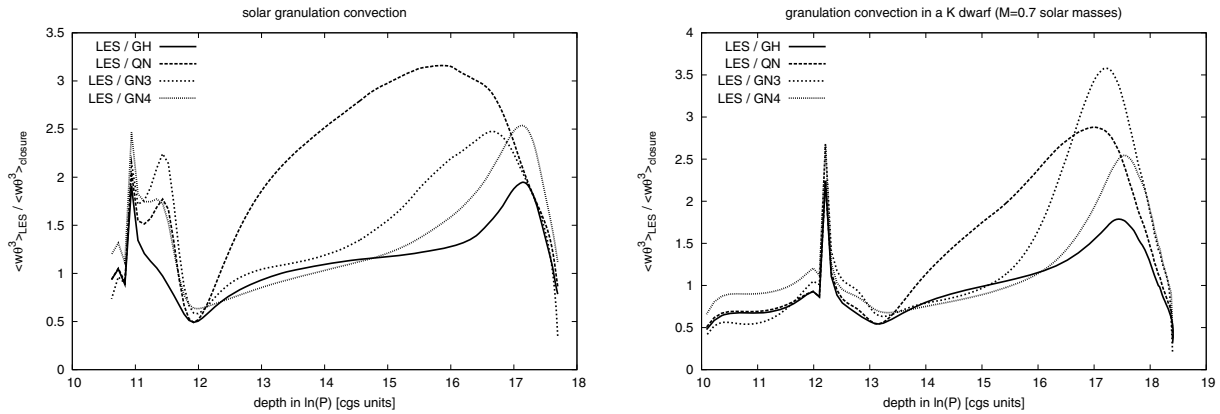

Figure 10. The ratios of $\overline{w\theta^3}$ computed from LES to different closures evaluated using the LES are shown for the case of the Sun (left-hand panel) and the K dwarf (right-hand panel).

in Table 1). It shares deviations of a factor of 2 around the superadiabatic peak for the Sun with all the other models, but also performs best in the photosphere. The GN3 model has much larger deviations in the quasi-adiabatic part of the convection zone, especially for the solar case, where a factor of 2 and more is common. The GN4 model performs better, but clearly not as good as the GH model and for $\overline{w^3\theta}$, it has the largest deviations where the correlation changes sign (around $\ln P \sim 11$ and $\sim$12.1 for the Sun and the K dwarf, respectively; the positive sign of the ratio indicates the change of sign occurs at the correct location in the models).

The different plots for $\overline{\theta^4}$ in Fig. 11 confirm that the conclusions drawn for $\overline{w\theta^3}$ are essentially correct. The ratio of the quasi-normal approximation to the direct computation is greater than 3 for the solar case and 2.5 for the K dwarf. Again in the superadiabatic zone, the FOM is overestimated by a factor of 2 and there are also similar sized discrepancies in the photosphere, at least in the solar case. Improvements obtained by the GH model are remarkable, as the discrepancies are reduced to less than 1.3 for both the solar and K dwarf case (excluding the lower boundary region below Z_3, where the model still performs better than the quasi-normal approximation – of course, this region is strongly influenced by the lower boundary conditions). Similar improvements are obtained for the photosphere for the solar case, but unfortunately not for the superadiabatic zone. The deviations for the GN3 model roughly follow the same pattern as in Fig. 10 for $\overline{w\theta^3}$. The model is not much of an improvement over the quasi-normal approximation and clearly worse than the GH model. The GN4 model performs slightly worse than the GH model. Its deviations are different, as it overestimates $\overline{\theta^4}$ in most of the quasi-adiabatic part of the convection zone.

4.3 Third-order moments

The two-scale mass-flux model of Gryanik & Hartmann (2002) yields expressions (22) and (23) for the TOMs $\overline{w^2\theta}$ and $\overline{w\theta^2}$. The linear scaling of all its ingredients with their Reynolds averages for the convective PBL (fig. 7 of Gryanik & Hartmann 2002) suggests that the high skewness limit (28) and (29) may hold for a much larger range of S_w and S_θ:

$$\overline{w^2\theta} = a_1\, S_w\, \sigma_w\, \overline{w\theta} = a_1\, \left(\overline{w^3}/\overline{w^2}\right)\, \overline{w\theta}, \tag{57}$$

$$\overline{w\theta^2} = a_2\, S_\theta\, \sigma_\theta\, \overline{w\theta} = a_2\, \left(\overline{\theta^3}/\overline{\theta^2}\right)\, \overline{w\theta}. \tag{58}$$

Remarkably, for the terrestrial case the factors a_1 and a_2 are found to be very close to 1 (table 2 and fig. 12 in Gryanik & Hartmann 2002). We hence tested equations (28) and (29) for both our solar granulation simulation and the simulation for the K dwarf in the same way as the expressions for the FOMs (Section 4.2). The right-hand side of equation (28) has been evaluated using the averages from the simulations and is compared to a direct (ensemble averaged) evaluation of $\overline{w^2\theta}$ in Fig. 12. Both sets of averages are normalized

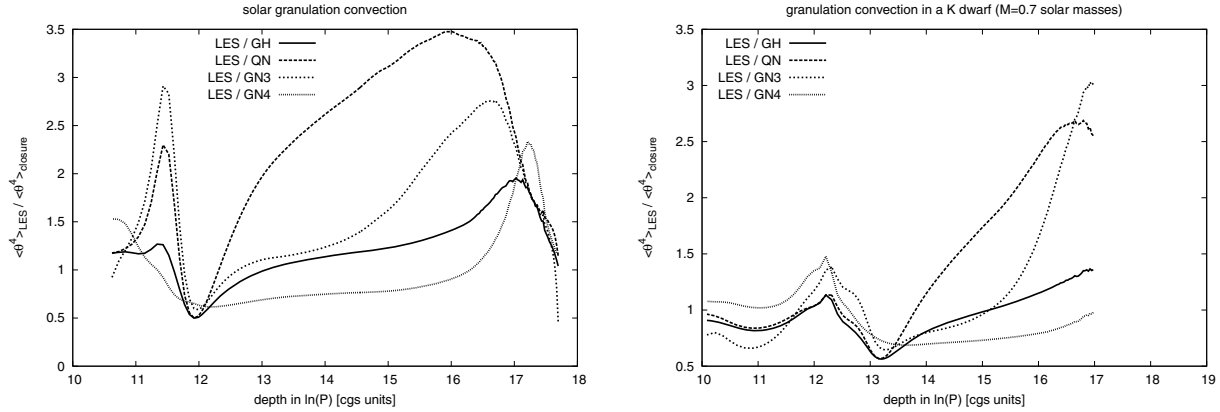

Figure 11. The ratios of $\overline{\theta^4}$ computed from LES to different closures evaluated using the LES are shown for the case of the Sun (left-hand panel) and the K dwarf (right-hand panel). The oscillations present in the bottom scaleheight for the solar case are small enough for a meaningful comparison. They are expected to disappear from even longer averaging. The same is not yet the case for the K dwarf, where averages of $\overline{\theta^4}$ for the bottom region ($\ln P > 17$) are not sufficiently converged to allow interpretation (they are the reason for the oscillations present in the data for K_θ in Fig. 3) and hence are not displayed.

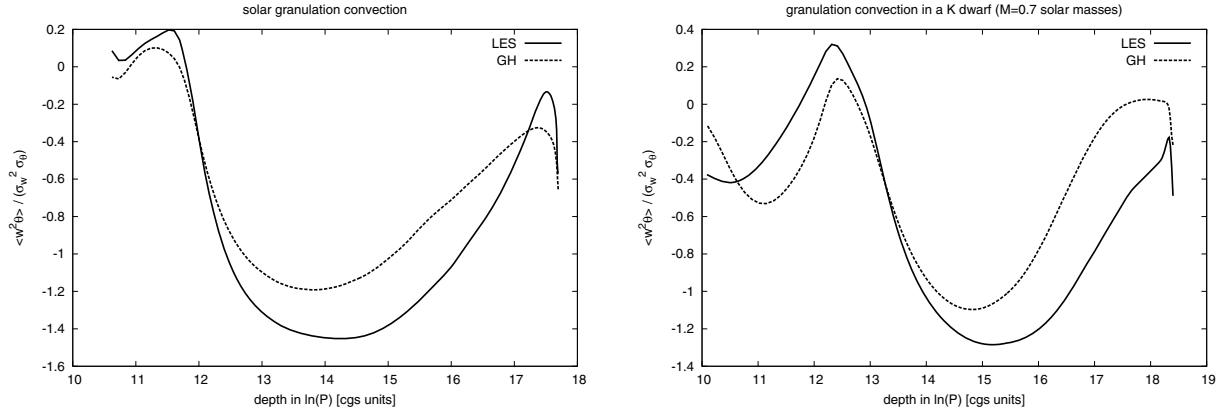

Figure 12. The left-hand panel compares $\overline{w^2\theta}$ normalized by $\sigma_w^2\sigma_\theta$ as obtained from LES with the two-scale mass-flux expression derived as a variant of the GH model for the case of the Sun, normalized and evaluated using the LES. The right-hand panel shows the same comparison for the K dwarf.

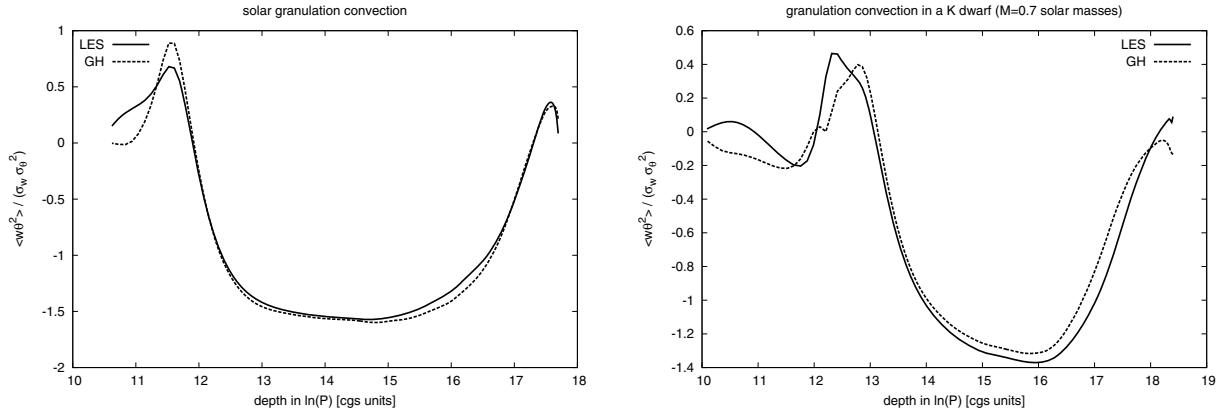

Figure 13. The left-hand panel compares $\overline{w\theta^2}$ normalized by $\sigma_w\sigma_\theta^2$ as obtained from LES with the two-scale mass-flux expression derived as a variant of the GH model for the case of the Sun, normalized and evaluated using the LES. The right-hand panel shows the same comparison for the K dwarf.

by the product $\sigma_w^2\sigma_\theta$, which is computed from the simulations. For the Sun, the agreement between model and data is better than for any of the models for FOMs. For the K dwarf, there are larger deviations near the bottom of the simulations and the deviations near the superadiabatic peak are more pronounced, although the overall agreement is still more satisfactory than those found for the various models of FOMs.

In Fig. 13, we present a similar comparison between the model expression (29) and direct averages for the solar and the K dwarf case for $\overline{w\theta^2}$, this time normalized to $\sigma_w\sigma_\theta^2$ as obtained from the

simulations. The agreement for the solar case is nearly perfect. Only in the atmosphere and the superadiabatic peak there is some room left for improvement. Remarkably, the agreement for the K dwarf is practically as good as for the solar case. Hence, model (29) is an excellent approximation for $\overline{w\theta^2}$.

It seems surprising that fluctuations within and in between the drafts do not lead to a more complicated dependence between two-scale mass-flux average and Reynolds average for $\overline{w^2\theta}$ and $\overline{w\theta^2}$. Improvements are mainly required in regions where $S_w \sim 0$ and $S_\theta \sim 0$. Following Zilitinkevich et al. (1999), who proposed a gradient (diffusion) type correction for equation (57) to improve results near the boundary between stable and unstable stratification, Gryanik & Hartmann (2002) suggested gradient terms to be added to the right-hand sides of both equations (57) and (58). We have investigated such corrections for the case of the solar convection simulation and found that small terms of type $d_1\tau\sigma_w^2\partial\overline{w\theta}/\partial z$ and $d_2\tau\sigma_w^2\partial\overline{\theta^2}/\partial z$, respectively, indeed allow a nearly perfect match of $\overline{w^2\theta}$ and $\overline{w\theta^2}$ near the superadiabatic peak, while maintaining the very good agreement for the quasi-adiabatic layers below unaltered.[3]

5 COMPARISON WITH OTHER STUDIES

In Grossman & Narayan (1993), SPH simulations were used to study models GN3 and GN4. A perfect gas was assumed as well as a prescribed radiative conductivity given as a function of depth. Peculiar boundary conditions had to be used to allow application of their simulation technique (particles are reflected, gravity is constant throughout most of the simulation box but approaches zero in the top and bottom boundary layers). Only the vertical direction was explicitly accounted for in their dynamical equations, while effects of horizontal flow had to be parametrized. They found models GN3 and particularly GN4 to be significant improvements over the quasi-normal approximation. Both models reduced rms differences between computations of FOMs directly from the SPH simulations and evaluations of the model equations with their simulations by typically a factor of 2 to 4. Qualitatively, model GN4 was found preferable over GN3, because it did a better job at reproducing regions for which correct symmetries with respect to sign change of θ are important. To our knowledge, models GN3 and GN4 have previously been tested only by their authors. As Figs 7–11 in Section 4.2 show, we find the same amount of improvement over the quasi-normal approximation of FOMs for both the solar and the K dwarf granulation simulations. In our case, for $\overline{w^2\theta^2}$, $\overline{w\theta^3}$ and $\overline{\theta^4}$, model GN4 is preferable over GN3. This is a consequence of its dependence on S_θ^2. The latter is not evident from equations (54)–(56), but taking into account the results of Section 4.3 which show how well $\overline{w^2\theta}$ and $\overline{w\theta^2}$ scale with S_w and S_θ, respectively, we conclude that the functional form assumed for model GN4 is equivalent to introducing a dependence of $\overline{w^2\theta^2}$ and $\overline{w\theta^3}$ on S_θ^2 (and of $\overline{w^2\theta^2}$ and $\overline{w^3\theta}$ on S_w^2). This can be seen from putting equations (57) and (58) into equations (54)–(56). Apart from an additional dependence on $C_{w\theta}^2$ which appears as a (height dependent) factor in front of the skewnesses, model GN4 then becomes quite similar to the GH model, both in functional form and overall performance. It also corroborates our claim in Section 3.3 that the functional form of the model expressions is more important than varying their coefficients by factors of the order of unity [1.5 for a_i in equation (40) and 2 for d_i in equation (41), as suggested by the numerical experiments in Gryanik & Hartmann 2002 and also, indirectly, in Grossman & Narayan 1993]. We note that in Grossman (1996) a modification of the dynamical equations underlying the SPH simulations of Grossman & Narayan (1993) was discussed. This modification explicitly accounts for a horizontal flow component. However, only a few tests of the quasi-normal approximation were presented which confirmed the previous results of Grossman & Narayan (1993).

Assuming the fully compressible Navier–Stokes equations in the large eddy (volume averaged) approximation for three spatial dimensions, Chan & Sofia (1996) performed numerical simulations of a deep convective atmosphere using a perfect gas equation of state and prescribed radiative conductivity. A convection zone almost 7 pressure scaleheights deep with nearly quasi-adiabatic stratification in its interior and a superadiabatic peak at its top, was embedded between two shallow stable layers located at the top and bottom. These layers separated the convection zone from the impenetrable stress-free boundaries. Numerous closure relations for lower order moments were studied by Chan & Sofia (1996) including the quasi-normal approximation. As can be seen in their fig. 11, the discrepancy between equations (11)–(15) and the direct evaluation of these FOMs is typically a factor of 2–3 within the interior (quasi-adiabatic) part of that convection zone. This is very close to what we find in Section 4.2 for the case of our solar granulation and K dwarf simulations. A related simulation run with a slightly larger stable layer on top than in the case presented in Chan & Sofia (1996) was made available to one of us (FK) by K. L. Chan. Again equations (11)–(15) underestimate the FOMs in the interior of the convection zone by a factor of 2–3. Likewise, the superadiabatic peak coincides with a region of small $|S_w|$ and small $|S_\theta|$, a maximum of $\overline{\theta^2}$ and $\overline{\theta^4}$, and low values of K_w and K_θ (slightly less than 2). This was also found for the solar and the K dwarf simulations (see Section 4.1). For that simulation, we have also verified that the GH model provides an even better improvement over the quasi-normal approximation: except for the region around the superadiabatic peak as well as the lower boundary of the convection zone deviations drop to a factor of less than 1.4 for $\overline{\theta^4}$ and less than a factor of 1.3 for the four other FOMs in the convectively unstable zone. Around the superadiabatic peak, the GH model essentially coincides with the quasi-normal approximation, while in the stably stratified layers the GH model again performs better than the quasi-normal approximation, reducing discrepancies by typically a factor of 2.

The GH model has also been compared to the quasi-normal approximation for two geophysical cases: one by Gryanik & Hartmann (2002) and Gryanik et al. (2005) for the case of three-dimensional numerical simulations and aircraft measurements of the PBL and another by Losch (2004) for numerical simulations for the ocean. Neither systems have the equivalent of a superadiabatic peak. The PBL can be subject to developing a shallow convection zone (typically 1/8 of a pressure scaleheight deep) with a stable temperature inversion layer on top (see also Garratt 1994). Possible causes include daytime heating of the ground under cloud-free conditions at negligible horizontal mean wind or a weak wind continuously moving cold air above a warmer surface. In both cases, radiative or conductive losses by the air itself are negligible. A weak wind moving cold air above a warm surface can give rise to a quasi-stationary convection zone. This is the scenario investigated by Gryanik & Hartmann (2002) and Gryanik et al. (2005). For the PBL, they showed the quasi-normal approximation (equations 11–15) suffers from systematic trends when predicting FOMs. The GH model avoids these trends. Moreover, explained variances as a measure of the mean

[3] The detailed values for the model constants d_1 and d_2 depend, among others, on how the turbulent dissipation time-scale τ is computed. For the solar simulation, the most simple prescription of taking τ to be a fraction of the local pressure scaleheight over $\sqrt{K}$, given by equation (1), was sufficient.

differences between data and model are improved by 15 per cent to 35 per cent compared to the quasi-normal approximation with explained variances attaining values of 92 per cent or better when compared to simulations instead of the previous 68 per cent (and at least 73 per cent compared to the previous 38 per cent for the aircraft measurements). This corresponds to improvements of a factor of 2 for each of the five FOMs. These conclusions hold for the lower three quarters of the PBL convection zone. Cheng, Canuto & Howard (2005) pointed out that measurements for the highest layers for which observational data were available indicate that the GH model underestimates K_w in that region. The same is not evident from the numerical simulations presented in Gryanik et al. (2005) with horizontal wind speed appropriate for the measurement conditions. Interestingly, for the lower 75 per cent of the PBL, K_w remains between 3 and 4.5. It increases as a function of height which is the opposite of the solar case, as in the PBL fast and narrow updrafts are enclosed by slow and broad downflows. Whether the high values for K_w of 5–6 are an indication for larger fluctuations within and between the upstreams near the top of the PBL or just result from insufficient averaging (horizontally and/or as a function of time) is yet unclear (cf. the large spread for K_θ in fig. 3 of Gryanik & Hartmann 2002).

The numerical simulations presented in Losch (2004) were used to study a case of oceanic deep convection. They assumed a convection zone spanning the entire vertical depth range between two impenetrable boundaries separated by 1 km (roughly 4.6 pressure scaleheights). For the bottom this approximation is excellent, while for the top it avoids dealing with the complex air–water interface which involves scales much smaller than that of the convective plumes and the chosen grid scale (10 m). Realistic microphysics was taken into account assuming a well-mixed medium. Three different cooling rates (which determine the convective driving) and three choices of Coriolis numbers (of the order of unity) were investigated. Both S_w and S_θ were found to attain values less than -1.5 within the top 10 per cent of the convection zone indicating realizability problems for the quasi-normal approximation in that region, as a result of equation (19). The negative skewnesses correspond to narrow and fast downwards moving plumes embedded in broad and slow upflows, just like our granulation simulations. With exception of $\overline{w^4}$ and for all cases studied, the quasi-normal approximation was found to yield poor results with systematic trends and low explained variances (between 23 and $\sim$85 per cent). Using the GH model provided improvements of a factor of 2–3 while removing most of the trends and increasing explained variances accordingly (to between 52 and 99 per cent). Only for $\overline{w^4}$ were the predictions of the quasi-normal approximation good enough so that the GH model was only able to provide minor additional improvements for the top layers. If one attempts a best fit of all cases studied by varying the parameters (equations 40–41) of equations (35)–(39), only minor improvements can be achieved (mostly for the case with weakest convection and slowest rotation/lowest Coriolis number). Those variations are of the same order as mentioned above (factors up to $\sim$1.5 for the a_i, somewhat larger for the d_i), but the small improvements gained from that procedure lack any universality, as the resulting numbers have no correlation with those found for the PBL case in Gryanik & Hartmann (2002). This again implies that optimizing the a_i and d_i with least-square fits to some data is not a worthwhile venture. Since a large number of additional tests were made by Losch (2004) to confirm the independence of these results from assumptions made about numerical and subgrid scale viscosity as well as other physical quantities, his studies were done for the case of only one horizontal direction in addition to the vertical one. Three-dimensional simulations had to be left for future work.

6 DISCUSSION AND CONCLUSIONS

6.1 Discussion

In Section 4, we showed that the improvements provided by the GH model for the quasi-adiabatic part of convection zones and its shortcomings near their boundaries are similar in both the solar and the K dwarf simulation of surface convection. The same is also found for a simulation with idealized microphysics as in Chan & Sofia (1996). In all these cases, the convection zones have a quasi-adiabatic stratification over several pressure scaleheights and a pronounced superadiabatic peak on its top. Apparently, these general properties are more important for the flow topology and for the behaviour of lower order moments, than the details of radiative cooling and effects due to ionization which distinguish our simulations from those of Chan & Sofia (1996). Our solar simulations are corroborated by a numerical simulation for solar granulation with open boundaries based on the code of Stein & Nordlund (1998) which is used in Belkacem et al. (2006a) to develop a closure model useful for the modelling of solar p-mode excitation rates (Belkacem et al. 2006b). For the bottom of the photosphere, the superadiabatic layer, and the top of the quasi-adiabatic part of the solar convection zone, both simulations are not only similar in their mean structure (cf. Section 2.1), but also agree within 20 per cent or better about the values for K_w, K_θ, $\overline{w^4}$, $\overline{\theta^4}$, S_w and S_θ (for $\overline{w^4}$ and the skewnesses, see figs 2 and 3 in Belkacem et al. 2006a).

Differences occur at the top of the photosphere and in the mid and lower part of the quasi-adiabatic convection zone and are caused by the boundary conditions. The closed lower boundary of our simulations leads to a drop of $K_w, K_\theta, S_w, S_\theta$ and related quantities towards values compatible with the impenetrable boundary, whereas they drop just slightly from their maximum values in the case of open boundaries (fig. 2 in Belkacem et al. 2006a). This is expected when deep downdrafts which continue further on, merge with each other, but otherwise within the nearly adiabatic environment the background conditions and the flow topology remain unaltered. As the astrophysically important differences between the FOM models discussed in Section 4 are established in the layers where simulations with deeply enough located closed and with open boundaries, respectively, agree closely, the conclusions we draw on the models are robust to the treatment of the simulation boundaries. This holds as long as the simulation boxes are deep and wide enough and have sufficient numerical resolution for the large-scale flows (see Robinson et al. 2003, and Section 2). We note that the simulations of Stein & Nordlund (1998) used in Belkacem et al. (2006a) are based on a non-grey treatment of radiative transfer while our own simulations use the grey approximation. For the study of lower order moment statistics of the bottom of the photosphere, the superadiabatic layer, and the quasi-adiabatic convection zone underneath, this difference is apparently unimportant.

The conclusions derived from our astrophysical convection simulations have also been found in simulations of the planetary convective boundary layer of the earth and in convection in the ocean (Section 5). The geophysical systems differ from the astrophysical case in many ways, such as in the microphysical properties of the fluids, in the heating and cooling mechanisms, boundary conditions and in the importance of stratification and compressibility. The main feature shared by the astrophysical and the geophysical cases is that of an interior, quasi-adiabatic convection zone with a filamentary

structure (plumes, updrafts or downdrafts) that results from the different areas being covered by up- and downflows and varying areas of fluid hotter and colder than the average. For that part of the convection zone, the quasi-normal approximation (equations 11–15) is found to be unsatisfactory in all cases presented in Section 4 and 5, while the GH model (equations 42–46) and in principle also the GN4 model (equations 52–56) are found to provide an improvement of up to an order of magnitude for the prediction of these quantities. We thus suggest that the shortcomings of the quasi-normal approximation and the improvements found for the alternative models are primarily caused by properties originating from the flow topology of convection found in each of these physical systems. This topology is characterized by coherent structures which, in the case of the Sun, emerge as granules and downdrafts at the top of its convection zone.

If we want to model the superadiabatic region of the Sun or a K dwarf, our tests with numerical simulations show that none of the models discussed in Section 4 is sufficient. The bright line in Fig. 1 indicates that the optical surface, the layers in which most of the observed radiation is emitted, is corrugated. Stein & Nordlund (1998) have shown that the fluid remains in radiative–convective equilibrium in the solar photosphere: although energy transport switches from convective to radiative at the surface, fluid parcels are both cooled and reheated once they have reached the surface. The extreme temperature sensitivity of opacity at the optical surface thus explains the location of the maxima of $\overline{\theta^2}$ and $\overline{\theta^4}$. The rapid increase in opacity at the solar surface leads to steep temperature gradients which peak where convection sets in as the dominant means of energy transport and where the corrugated optical surface causes the maxima in $\overline{\theta^2}$ and $\overline{\theta^4}$. As discussed in Section 4.1, the radiative exchange also leads to a drop of K_w and K_θ to values between 1.5 and 2, well below the value of 3 obtained for a quasi-normal distribution. This effect clearly has to operate on the level of individual drafts, as the corrugated optical surface cannot sufficiently constrain K_w and K_θ on its own. Density fluctuations of the highly compressible flow further enhance this drop. For instance, fluid in the updraft which cools more rapidly than at its adiabatic expansion rate and which remains in pressure equilibrium with its environment will experience further cooling and large excess temperature fluctuations within the draft will be damped more efficiently, thus lowering K_θ. The increased radiative exchange and turnover of fluid due to loss of buoyancy likewise leads to a drop in $|S_w|$ and $|S_\theta|$ and explains the coincidence of minima of K_w and K_θ with $S_w \sim 0$ and $S_\theta \sim 0$. As a result, both kurtosis and skewness are quite different from what is assumed in the picture underlying local convection models, both in the quasi-adiabatic part of the convection zone and in the superadiabatic layer. The elaborated physical picture required to explain the behaviour of skewness and kurtosis suggests that these are useful quantities for describing the effects of large-scale coherent structures on the distributions of velocities and temperatures observed in solar and stellar surface convection.

6.2 Conclusions and outlook

The results discussed in Sections 4 and 5 show that the quasi-normal approximation can only give an order of magnitude estimate for the one-point Reynolds averages of FOMs of vertical velocity and temperature. Taking into account that the main assumptions underlying this approximation are homogeneity, isotropy and uncorrelatedness of the fields being averaged, the low accuracy of equations (11)–(15) is mainly the result of the non-locality of turbulent convection and of the coherently organized structures which perform most of the transport provided by this type of flow. To improve on equations (11)–(15), mass-flux models and expansions in terms of skewness have been proposed. As a comparison of equations (42)–(46) with equations (52)–(56) shows, both approaches can lead to algebraically similar extensions of equations (11)–(15). The detailed comparison of the models with numerical simulations of granulation in the Sun and a K dwarf shows that the correct symmetries with respect to temperature and velocity are important. For exactly that reason, the GN3 model falls clearly short of the GH and the GN4 model when we compare predictions of $\overline{w^2\theta^2}$, $\overline{w\theta^3}$ and $\overline{\theta^4}$ with simulation data.

The differences between the GH and the GN4 model are much smaller, as we can see from the results for the solar and the K dwarf simulations presented in Section 4.2. They have the same size as if we had varied the coefficients (equations 40–41) of equations (35)–(39) by factors of about 1.5–2. This immediately follows from comparing equations (42)–(46) and equations (28)–(29) with equations (52)–(56). From that point of view, a preference for the GH model based on smaller maximum differences from directly computed FOMs or better results for $\overline{w\theta^3}$ as selection criteria, may appear a bit arbitrary. We think it is more important that individual optimizations of equations (40) and (41) are found to be specific to particular physical problems and thus lack universality. This follows from the results discussed in Section 5, if the optimum fit parameters of Gryanik & Hartmann (2002) are compared with those found by Losch (2004) and those implied by equations (52)–(56). The choice of equations (40) and (41) taken for equations (42)–(46) is found in the middle of this range of best-fitting parameters. Moreover, the GH model also fulfils an asymptotic limit for the case of very high skewness (which the GN models do not), even though the limit may not be attained in stellar convection zones. From that point of view, the GH model appears preferable over the GN4 one. We finally recall that while the numerical simulations themselves, the GH model (and also the two-scale mass-flux model of Gryanik & Hartmann 2002), as well as the GN4 model pass the realizability test (19), both the GN3 model and the quasi-normal approximation fail.

In light of the variety of tests also done in neighbouring fields (cf. Section 5), we conclude that the GH model (equations 42–46) together with equations (28) and (29) is the most appropriate one to improve predictions of TOMs and FOMs of vertical velocities and temperature as a function of SOMs and skewness in the interior, quasi-adiabatic region of convection zones (at points sufficiently away from upper and lower boundaries). In that region, the model allows predictions with a typical accuracy of 20–30 per cent instead of the order of magnitude estimates provided by the quasi-normal approximation. We note that the latter, however, can still be expected to be useful when closing FOMs of horizontal velocity components in terms of second-order ones (Section 4.1). In the quasi-adiabatic part of the convection zone, the model (42)–(46) could help to improve Reynolds stress convection models as well as the modelling of p-mode excitation in solar type and other cool dwarf stars. The latter has already been investigated (Belkacem et al. 2006a, b). The extra energy injected into those solar p modes, which have significant contributions to their excitation from the top of the quasi-adiabatic part of the solar convection zone, is indeed found to provide major improvements when comparing theory with observations (Belkacem et al. 2006b).

The GH and GN4 models performed poorly only in transition regions, such as the capping region at the top of the PBL or the radiation/convection transition region at the top of the solar convection zone. In the case of the Sun and other cool stars such as K dwarfs, the transition region is characterized by complex radiative exchange in the flow which can only be accounted for by a

more complete physical model. Eddy damping methods applied to the quasi-normal approximation, as described in Section 3.2, have to face exactly the same challenge. While results for some cases (Kupka & Montgomery 2002; Montgomery & Kupka 2004) appear encouraging, a model of general applicability for solar and stellar convection may require a much more detailed picture of radiative transfer and flow topology. In that case, models like those of Gryanik & Hartmann (2002) and Gryanik et al. (2005) certainly provide a promising starting point.

ACKNOWLEDGMENTS

FK would like to express his gratitude to V. M. Canuto and V. M. Gryanik for numerous discussions on their turbulence models and K. L. Chan for providing simulation data for a deep convection zone with idealized microphysics.

REFERENCES

Alexander D. R., Ferguson J. W., 1994, ApJ, 437, 879
André J. C., De Moor G., Lacarrère P., du Vachat R., 1976a, J. Atmos. Sci., 33, 476
André J. C., De Moor G., Lacarrère P., du Vachat R., 1976b, J. Atmos. Sci., 33, 482
Arakawa A., 1969, Proc. WMO/IUGG Symp. Numerical Weather Prediction, Parametrization of Cumulus Convection. Japan Meteorological Agency, Japan IV, 8, p. 1
Arakawa A., Schubert W. H., 1974, J. Atmos. Sci., 31, 674
Asplund M., Ludwig H.-G., Nordlund Å., Stein R. F., 2000, A&A, 359, 669
Belkacem K., Samadi R., Goupil M. J., Kupka F. 2006a, A&A, in press (DOI: 10.1051/0004-6361:2006.5369)
Belkacem K., Samadi R., Goupil M. J., Kupka F., Baudin F., 2006b, A&A, in press (DOI: 10.1051/0004-6361:2006.5370)
Blanchet J., 1970, Etude statistique d'un système fluide. Application à la météorologie, in La Météorologie V, 15, 15
Böhm-Vitense E., 1958, Z. Astrophys., 46, 108
Canuto V. M., 1992, ApJ, 392, 218
Canuto V. M., 1993, ApJ, 416, 331
Canuto V. M., 1997, ApJ, 482, 827
Canuto V. M., Dubovikov M., 1998, ApJ, 493, 834
Canuto V. M., Mazzitelli I., 1991, ApJ, 370, 295
Canuto V. M., Minotti F., Ronchi C., Ypma R. M., Zeman O., 1994, J. Atmos. Sci., 51, 1605
Canuto V. M., Goldman I., Mazzitelli I., 1996, ApJ, 473, 550
Canuto V. M., Cheng Y., Howard A., 2001, J. Atmos. Sci., 58, 1169
Chan K. L., Sofia S., 1996, ApJ, 466, 372
Chan K. L., Wolff C. L., 1982, J. Comput. Phys., 47, 109
Cheng Y., Canuto V. M., Howard A. M., 2005, J. Atmos. Sci., 62, 2189
Cox J. P., Giuli R. T., 1968, Principles of Stellar Evolution. Gordon & Breach Science Publishers, New York
Frenkiel F. N., Klebanoff P. S., 1967, Phys. Fluids, 10, 1737
Garratt J. R., 1994, The Atmospheric Boundary Layer. Cambridge Univ. Press, Cambridge
Grossman S. A., 1996, MNRAS, 279, 305
Grossman S. A., Narayan R., 1993, ApJS, 89, 361
Gryanik V. M., Hartmann J., 2002, J. Atmos. Sci., 59, 2729
Gryanik V. M., Hartmann J., Raasch S., Schröter M., 2005, J. Atmos. Sci., 62, 2632
Guenther D. B., 1994, ApJ, 422, 400
Hanjalić K., Launder B. E., 1972, J. Fluid Mech., 52, 609
Iglesias C. A., Rogers F. J., 1996, ApJ, 464, 943
Kuhfuss R., 1986, A&A, 160, 116
Kupka F., 2005a, in Kupka F., Hillebrandt W., eds, Proc. MPA/P15, Interdisciplinary Aspects of Turbulence. MPI for Astrophysics, Garching, p. 141
Kupka F., 2005b, in Alecian G., Richard O., Vauclair S., eds, EAS Publications Ser., Vol. 17, Element Stratification in Stars: 40 Years of Atomic Diffusion. EDP Sciences, Les Ulis, p. 177
Kupka F., 2007, in Kupka F., Roxburgh I. W., Chan K. L., eds, Proc. IAU Symp. 239, Convection in Astrophysics. Cambridge Univ. Press, Cambridge, in press
Kupka F., Montgomery M. H., 2002, MNRAS, 330, L6
Kupka F., Muthsam H. J., 2007, in Kupka F., Roxburgh I. W., Chan K. L., eds, Proc. IAU Symp. 239, Convection in Astrophysics. Cambridge Univ. Press, Cambridge, in press
Losch M., 2004, Geophys. Res. Lett., 31, L23301
Lumley J. L., Zeman O., Siess J., 1978, J. Fluid Mech., 84, 581
Millionshchikov M. D., 1941, Dokl. Akad. Nauk SSSR, 32, 615
Mironov D. V., Gryanik V. M., Lykossov V. N., Zilitinkevich S., 1999, J. Atmos. Sci., 56, 3478
Montgomery M. H., Kupka F., 2004, MNRAS, 350, 267
Orszag S. A., 1970, J. Fluid Mech., 41, 363
Petersen A. C., Beets C., van Dop H., Duynkerke P. G., Siebesma A. P., 1999, J. Atmos. Sci., 56, 37
Randall D. A., Shao Q., Moeng C.-H., 1992, J. Atmos. Sci., 49, 1903
Robinson F. J., Demarque P., Li L. H., Sofia S., Kim Y.-C., Chan K. L., Guenther D. B., 2003, MNRAS, 340, 923
Rosenthal C. S., Christensen-Dalsgaard J., Nordlund Å., Stein R. F., Trampedach R., 1999, A&A, 351, 689
Siebesma A. P., Cuijpers J. W. M., 1995, J. Atmos. Sci., 52, 650
Stein R. F., Nordlund Å., 1998, ApJ, 499, 914
Xiong D. R., 1980, Chin. Astron., 4, 234 (Original in Chinese inXiong D. R., 1979, Acta Astron. Sin., 20, 238)
Xiong D. R., Cheng Q. L., Deng L., 1997, ApJS, 108, 529
Zeman O., Lumley J. L., 1976, J. Atmos. Sci., 33, 1974
Zilitinkevich S., Gryanik V. M., Lykossov V. N., Mironov D. V., 1999, J. Atmos. Sci., 56, 3463

This paper has been typeset from a TEX/LATEX file prepared by the author.